

國 立 交 通 大 學

環 境 工 程 研 究 所

博 士 論 文

背斜受限含水層中定流量抽水試驗之解析洩降解

An Analytical Drawdown Solution for Constant-flux

Pumping in a Confined Anticline Aquifer

研 究 生：陳 彥 如

指 導 教 授：葉 弘 德

中 華 民 國 九 十 九 年 八 月

背斜受限含水層中定流量抽水試驗之解析洩降解
An Analytical Drawdown Solution for Constant-flux
Pumping in a Confined Anticline Aquifer

研究生：陳彥如

Student：Yen-Ju Chen

指導教授：葉弘德

Advisor：Hund-Der Yeh



A Dissertation
Submitted to Institute of Environmental Engineering
College of Engineering
National Chiao Tung University
in Partial Fulfillment of the Requirements
for the Degree of
Doctor of Philosophy
in
Environmental Engineering
August, 2010
Hsinchu, Taiwan

中華民國九十九年八月

背斜受限含水層中定流量抽水試驗之解析洩降解

研究生：陳彥如

指導教授：葉弘德

國立交通大學環境工程研究所

摘 要

背斜地層是岩層受力彎曲後，形成向上拱起的褶皺地層。結構完整的背斜地層，可能作為廢棄物地下貯存或二氧化碳封存的場所。定流量抽水試驗藉由量測和分析觀測井的洩降反應，推求含水層的水文地質參數。本研究建立一個數學模式，用以描述定流量抽水試驗到達穩態時，背斜水層內的洩降分佈。在推導過程中，首先用三塊相連的長方體，近似模擬背斜地層的空間形體，接續採用傅立葉轉換和有限傅立葉餘弦轉換，推導得到轉換域的解後，進行傅立葉逆轉換以計算空間洩降的分佈值。使用此解進行模擬的結果，顯示兩翼較薄或是背脊較窄的水層，在井周圍會產生較大的洩降值。此外，在相同的抽水率條件下，縮減濾管開口長度和水層的異向性，會增加靠近井緣的無因次洩降。考慮不同設井位置的影響時，部分貫穿井若位於背斜脊中央上段處，在井周圍會產生較大的洩降。採用MODFLOW 模擬地下水流時，取用適當的格網可近似模擬背斜形狀。與解析解結果相比，MODFLOW 模擬結果所產生的洩降值較小。本研究所提出的解析解，也可應用於模擬平板形水層和斜坡水層的洩降分佈，將來亦可應用來逆推背斜含水層的水文地質參數值或做為廢棄物地下貯存場址篩選、設計的參考。

關鍵字：背斜含水層，抽水試驗，部分貫穿井，異向性，積分轉換

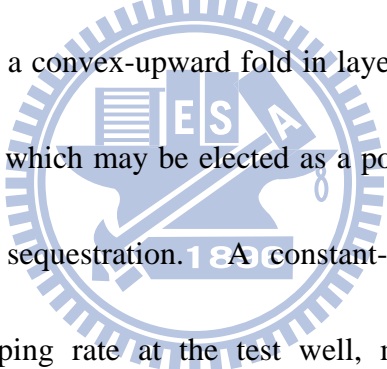
An Analytical Drawdown Solution for Constant-flux Pumping in a Confined Anticline Aquifer

Student : Yen-Ju Chen Adviser : Hund-Der Yeh

Institute of Environmental Engineering

National Chiao Tung University

ABSTRACT



An anticline known as a convex-upward fold in layers of rock commonly forms during lateral compression, which may be elected as a potential site for underground waste storage or carbon sequestration. A constant-flux pumping test, which maintains a constant pumping rate at the test well, measures and analyzes the drawdown responses in one or several observation wells to determine the aquifer parameters. In this study, a mathematical model is developed for describing the steady-state drawdown distribution in the anticline aquifer during the constant-flux pumping. In the derivation, the topographical shape of the anticline is mimicked by three successive blocks. The infinite Fourier transform and finite Fourier cosine transform are applied to obtain the solution of the model in the transform spaces. The solution expressed as an integral form is then obtained from the Fourier inversion.

Predicted results from the solution reveal that a thin-limbs or narrow-ridged anticline would cause a much larger head drop in the ridge zone. For a well of constant pumping rate, the dimensionless drawdown around the well increases with decreasing well screen length or/and aquifer anisotropy ratio. In examining the effect of well location, we find the partially penetrating well located at the top-middle of the ridge zone produces the largest drawdown. MODFLOW is a computer program that simulates the groundwater flow based on the block-centered finite difference method. Through the grid discretization, MODFLOW can imitate the antiform much closer to reality. The simulation for the flow in an anticline aquifer results in slightly smaller drawdown values when compared with those predicted by the present solution. The present solution can also be used to simulate the flow in a slab-shaped aquifer or a hillslope aquifer. It can be applied to identify the aquifer parameters and to design a potential site for waste disposal in the future as well.

KEYWORDS: anticline aquifer, pumping test, partially penetrating well, anisotropy, integral transform

誌 謝

本論文承蒙指導教授葉弘德博士，悉心指導與鼓勵，得以順利完成，特此表達我誠摯的謝意。老師嚴謹治學的態度、鍥而不捨的精神是我輩學習的典範。此外，本論文的完成亦得感謝感謝台灣大學劉振宇教授、中國科技大學陳主惠教授、中興大學謝平城教授、交通大學葉立明教授四位口試委員，對本論文的細心指正和寶貴意見，使內容更加充實完整，並且讓我獲益良多。

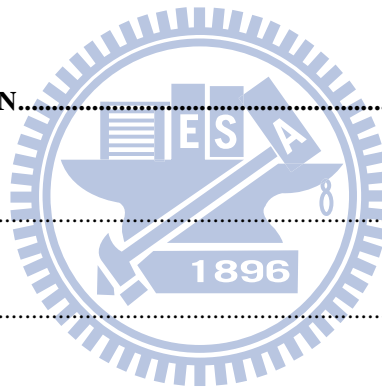
由衷感謝研究室智澤學長與彥禎學長在各方面的指點與幫助，特別感謝雅琪學姐在我碩、博士班其間的陪伴，給予寶貴的意見、支持及關懷。另外，眾位學弟妹敏筠、毓婷、士賓、博傑、其珊、琬儀、仲豪、庚轅、璟勝、昭志、國豪、及裕霖，你們讓我的博士研究生活，更添樂趣和歡笑。至誠的支持、體諒及幫忙更是我前進的動力。

最後將此論文獻給我的家人。感謝他們在我異鄉求學時，總是默默的給予支持與包容，我才能順利完成博士學業。也將此論文獻給所有關心我的朋友們，並致上我最真誠的敬意與謝意。

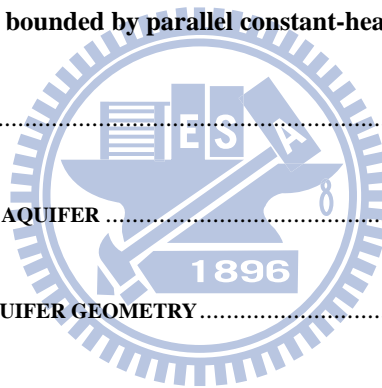
彥如 謹致於
交通大學環境工程研究所
2010年8月

TABLE OF CONTENTS

中文摘要.....	I
ABSTRACT	II
誌謝	IV
TABLE OF CONTENTS	V
LIST OF FIGURES.....	VIII
LIST OF NOTATIONS	XI
CHAPTER 1 INTRODUCTION.....	1
1.1 BACKGROUND	1
1.2 LITERATURE REVIEW	2
1.3 OBJECTIVE	5
CHAPTER 2 METHODOLOGY.....	6
2.1 MATHEMATICAL MODELING OF THE FLOW PROBLEM	6
2.1.1 Formulation for flow in zone 1.....	7
2.1.2 Formulation for flow in zone 2.....	9
2.1.3 Formulation for flow in zone 3.....	10
2.2 ANALYTICAL SOLUTIONS.....	11
2.2.1 Dimensionless drawdown solutions for zones 2 and 3.....	11



2.2.2 Dimensionless drawdown solution for zone 1	13
2.3 NUMERICAL EVALUATIONS	16
2.3.1 Calculation on Eqs. (22), (26), (38), and (39)	16
2.3.2 Inverse Fourier Transform	17
2.4 NUMERICAL SIMULATIONS IN MODFLOW	17
CHAPTER 3 RESULTS AND DISCUSSION	19
3.1 SPECIAL CASES	19
3.1.1 Slab-shaped aquifer bounded by parallel constant-head boundaries	19
3.1.2 Hillslope aquifer	21
3.2 BASE CASE OF ANTICLINE AQUIFER	22
3.3 EFFECT OF ANTICLINE AQUIFER GEOMETRY	26
3.4 EFFECT OF WELL PARTIAL PENETRATION	26
3.4.1 Effect of screen length and aquifer anisotropy	26
3.4.2 Effect of penetration ratio	28
3.4.3 Effect of well location	29
CHAPTER 4 CONCLUSIONS	31
REFERENCES	34
APPENDIX A DERIVATION OF EQ. (22)	38



APPENDIX B MATRIX FORMULATION FOR SOLVING COEFFICIENTS39

VITA (作者簡歷)53

PUBLICATION LIST54



LIST OF FIGURES

Figure 1. Schematic representation of a groundwater flow problem in an anticline aquifer with a line sink located along the z axis. The anticline aquifer is approximately divided into three blocks.....41

Figure 2. The dimensionless drawdown distributions predicted by the present solution and the image-well method (Ferris et al., 1962) for pumping at the middle of a slab-shaped aquifer bounded by two parallel constant-head boundaries.....42

Figure 3. Dimensionless drawdown contours and flow field for the pumping at a fully penetrating well in a hillslope aquifer. The simulations were carried out to a step-like aquifer by (a) the present solution, (b) MODFLOW, (c) MODFLOW with multiple steps to approximate the inclined boundary.....43

Figure 4. Dimensionless drawdown contours produced by the present solution for the pumping at a fully penetrating well in an isotropic anticline aquifer. The cross-sectional view on (a) $x_D - z_D$ plane for $y_D = 0$, (b) $y_D - z_D$ plane for $x_D = 0.2$, and (c) $y_D - z_D$ plane for $x_D = 0.8$ 44

Figure 5. Dimensionless drawdown contours produced by MODFLOW for the pumping at a fully penetrating well in an isotropic anticline aquifer. The

applied aquifer geometry is the same as that in Figure 4. The cross-sectional view on (a) $x_D - z_D$ plane for $y_D = 0$, (b) $y_D - z_D$ plane for $x_D = 0.2$, and (c) $y_D - z_D$ plane for $x_D = 0.8$ 45

Figure 6. Dimensionless drawdown contours produced by MODFLOW for the pumping at a fully penetrating well in an isotropic anticline aquifer. The upper boundary of anticline aquifer is approximated by multiple steps. The cross-sectional view on (a) $x_D - z_D$ plane for $y_D = 0$, (b) $y_D - z_D$ plane for $x_D = 0.2$, and (c) $y_D - z_D$ plane for $x_D = 0.8$ 46

Figure 7. Plots of dimensionless drawdown contours and flow fields for pumping at a fully penetrating well in an isotropic aquifer of (a) thin limbs and (b) narrow ridge.....47

Figure 8. Dimensionless drawdown responses versus x_D calculated at $(y_D, z_D) = (0, 1)$ for the base case shown in Figure 4 and the cases investigated in Figure 7.....48

Figure 9. A comparison of largest dimensionless drawdown at $(x_D, y_D) = (0.001, 0)$ for the cases of different screen length and aquifer anisotropy ratios. The wells are screened from the top-middle of the anticline aquifer. The geometry of the aquifer is the same as the base case shown in Figure 4.....49

Figure 10. Plots of dimensionless drawdown contours and flow fields for the pumping at a partially penetrating well in the aquifers with the anisotropy ratios of (a) $\chi_{zx} = 0.3$ and (b) $\chi_{zx} = 3$. The dimensionless screen length of the pumping well is 0.2.50

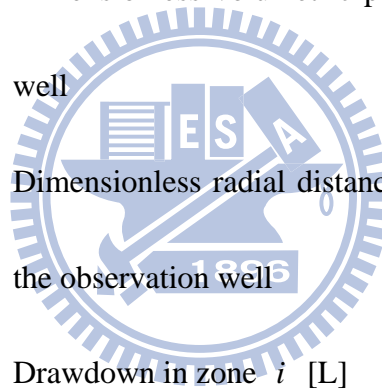
Figure 11. Plots of dimensionless drawdown contours for the pumping at partially penetrating wells in an aquifer with the dimensionless screen lengths of (a) $z_{Dl} = 0.8$, (b) $z_{Dl} = 0.857$ and (c) $z_{Dl} = 0.914$. The wells are located at a dimensionless x_D distance of 0.25 from the midline of the anticline aquifer.....51

Figure 12. Plots of dimensionless drawdown contours and flow fields for the pumping at a partially penetrating well with the dimensionless screen length of 0.2. The wells are located at (a) $z_{0D} = 1.0$ and (b) $z_{0D} = 0.2$ on the midline of the anticline aquifer and (c) $z_{0D} = 0.8$ at a dimensionless x_D distance of 0.25 from the midline of the anticline aquifer.....52

LIST OF NOTATIONS

a_i	Distance from the origin to the outer boundary of zone i in x -direction [L]
A_n	Function of x_D defined by Eq. (23)
b_i	Height of zone i [L]
B_k	Function of x_D defined by Eq. (27)
$C_{1m}, C_{2m}, C_{4m}, C_{6m}, C_{7m}$	Functions of x_D defined by Eq. (41), (42), (44), (46), and (47), respectively
$C_{3n}, C_{5k}, C_{8m}, C_{9m}$	Constants defined by Eqs. (43), (45), (B22), and (B23), respectively
$D_{00}, D_{0i}, D_{n0}, D_{ni}$	Constants defined by Eqs. (B2), (B3), (B4), and (B5), respectively
$E_{00}, E_{0j}, E_{n0}, E_{nj}$	Constants defined by Eqs. (B6), (B7), (B8), and (B9), respectively
$F_{00}, F_{0i}, F_{k0}, F_{ki}$	Constants defined by Eqs. (B10), (B11), (B12), and (B13), respectively
$G_{00}, G_{0j}, G_{k0}, G_{kj}$	Constants defined by Eqs. (B14), (B15), (B16), and (B17), respectively
k_x, k_y, k_z	Hydraulic conductivities in the x , y and z

	directions, respectively [L/T]
l	Screen length [L]
P_1, P_2	Undetermined coefficients in Eq. (A2)
q	Volumetric pumping rate per unit length of the pumping well [L ² /T]
q_D	Dimensionless volumetric pumping rate per unit length of the pumping well
Q_D	Dimensionless volumetric pumping rate of the pumping well
r_D	Dimensionless radial distance from the pumping well to the observation well
s_i	Drawdown in zone i [L]
s_{Di}	Dimensionless drawdown in zone i
\bar{s}_{Di}	Dimensionless drawdown for zone i in Fourier domain
$\hat{s}_{D1P}, \hat{s}_{D1N}$	Dimensionless drawdown for zones 1P and 1N in Fourier and Finite Fourier cosine domain, respectively
S	Storativity of the aquifer
S_0, S_n	Constants defined by Eqs. (B18) and (B19)
t_D	Dimensionless time defined by Eq. (57)



T	Transmissivity of the aquifer [L^2/T]
T_0, T_k	Constants defined by Eqs. (B20) and (B21)
u_p, u_{im}, u_{in}	Dimensionless variables in well functions, defined by Eqs. (54), (55), and (56), respectively
U	Unit step function
U_c, U_{c0}, U_{cm}	Constants defined by Eq. (32)
V_0, V_n, W_0, W_k	Coefficients in Eqs. (22), (26), (38), and (39), respectively
W	well function
x_0, y_0, z_0	Coordinate of the top point of the pumping well
x_{0D}, y_{0D}, z_{0D}	Dimensionless coordinate of the top point of the pumping well
x_D, y_D, z_D	Dimensionless coordinate variables
x_{Dai}	Dimensionless x -direction distance from the origin to the outer boundary of zone i
z_{Dbi}	Dimensionless height of zone i
z_{Dl}	Dimensionless screen length of the pumping well
α_n	Constant defined by Eq. (24)
β_k	Constant defined by Eq. (28)

χ_{yx}, χ_{zx}	Anisotropy ratios
δ	Dirac delta function
ε	Fourier transform variable
$\phi(m, n)$	Constant defined by Eq. (48)
γ_m	Constant defined by Eq. (40)
λ_m	Finite Fourier cosine transform variable used with respect to Eq. (1) and defined by Eq. (31)
θ	Angle between the positive x_D -axis and the line connecting the pumping and observation well
$\mathcal{G}(m, k)$	Constant defined by Eq. (49)
ω_n	Finite Fourier cosine transform variable used with respect to Eq. (10) and defined by Eq. (25)
ζ_k	Finite Fourier cosine transform variable used with respect to Eq. (16) and defined by Eq. (29)

CHAPTER 1 INTRODUCTION

1.1 Background

In structural geology, an anticline, as a result of lateral compression in crustal deformation, is a convex-upward fold in layers of rock. A well-structured anticline formation may be considered as a potential site for waste disposal or carbon sequestration. Ashjari and Raeisi (2006) investigated the groundwater flow in Zagros anticlines in Iran and indicated that the anticline structure of aquifers and the geometry of bedrocks primarily dominate the direction of regional groundwater flow. Moreover, it can be expected that the flow patterns will be changed on the condition that wastes or water being injected into or pumped from the aquifer. Because of the movement of groundwater carries the contaminants, explicit information such as geological structure and hydrogeological data are necessary to judge the applicability of the potential storage sites or to predict the migration of the contaminant plume in the site.

The drawdown or head data set obtained from a field aquifer testing, e.g., slug test or pumping test, is generally analyzed based on a relevant solution to determine the aquifer parameters. For a constant-flux pumping test, the test well pumps at a constant flow rate during the test time and the drawdown responses are measured in one or more observation wells in the vicinity. Commonly, a drawdown solution is

either incorporated with an optimization technique or applied to generate the type curves for the graphical method to find the best-fit aquifer parameters. An anticline aquifer has curved surfaces on their top and bottom boundaries; moreover, its profile may be asymmetric to its ridge. The complexity of the geometric situation of an anticline makes it challenging to solve the model analytically. In this study, we devoted to derive the analytical solution for the drawdown distribution in the approximated anticline aquifer since it can serve as an invaluable tool for gaining physical insight into the flow behavior affected by geologic and geometric settings.

1.2 Literature Review

The classic Thiem (1906) or Theis (1935) equation may be the most popular way used to estimate the drawdown distribution or to determine the aquifer parameters in an inverse problem for a constant-flux pumping in a confined aquifer. The Thiem equation (1906) described the spatial drawdown distribution within the radius of influence under steady-state condition. The Theis solution (1935) delineated the transient drawdown response in a confined aquifer. However, the assumptions made for developing these equations on well of full penetration and aquifer of infinitely lateral extent may not be capable of describing the flow in an anticline aquifer. Numerous studies have been made to cope with the groundwater flow problem edged

with peculiar boundaries. Among these studies, the integral transform method is commonly used to obtain the hydraulic head or drawdown solutions for specific boundary conditions in the mathematical model. For example, Chan et al. (1976) used the finite Fourier transform to obtain the transient and steady-state drawdown solutions for pumping in a rectangular aquifer. Chan et al. (1978) and Yeh and Chang (2006) applied the finite sine transform and Hankel transform to obtain the transient and steady-state analytical solutions for head distribution in a wedge-shaped aquifer. On the other hand, some drawdown solutions accounting for various topography boundaries in flow systems are based on the image-well method. The method removes aquifer boundaries and place pumping or recharging image wells at judicious locations. The drawdown in an observation well is calculated by summing up the drawdown or buildup due to the real well and image wells (Ferris et al. 1962; Streltsova 1988; Kuo et al. 1994; Chen et al. 2009).

The domain decomposition method can be applied to handle the problem with complex geometry or mix-typed boundary. In this method, the problem domain is split into several subdomains. Thereafter, the solutions for each subdomain are derived to satisfy the corresponding boundary conditions as well as the continuities of head and flux at the interface between the connected elements. The concept of domain decomposition method was first presented in Kirkham (1957) to calculate the

electrostatic potential between two concentric coaxial capped cylinders. The procedure was further extended in Kirkham (1959) to obtain the hydraulic head solution for the flow toward a partially penetrating well in a confined aquifer. Later, Javandel and Zaghi (1975) used a similar procedure to obtain the potential distribution in a confined aquifer due to the pumping at a well of vertically full penetrating and radially finite extension on the bottom of the aquifer. A similar decomposition concept was also deployed by Connell et al. (1998) for solving the problem of topographically driven flow in hillslope aquifers by dividing the problem domain into several rectangular elements.

Recently, some studies using numerical or analytical approaches were presented to investigate the head responses in anticline reservoirs due to the well injection or pumping. Al-Mohannadi et al. (2007) used the finite-difference method to simulate the transient pressure responses to horizontal wells in anticline reservoirs and curved wells in slab reservoirs. Yeh and Kuo (2010) proposed a steady-state analytical solution for a constant-head injection via a fully penetrating well into a heterogeneous, anisotropic, and dome-like anticline reservoir. Yet, it seems to lack the consideration of well partial penetration and asymmetric profile of the anticline.

1.3 Objective

The objective of this study is to develop a mathematical model for describing the steady-state drawdown distribution to a constant-flux pumping in an anticline aquifer. The pumping well is of infinitesimal diameter and can partially or fully penetrate the aquifer. The anticline aquifer is homogeneous, anisotropic and confined by a curved layer on the top and a horizontal impermeable layer at the bottom. Three successive blocks of different heights are used to represent the shape of the top curved boundary. The solution of the model is then obtained by applying the integral transform techniques including Fourier transform (FT) and finite Fourier cosine transform (FFCT) within each block and the hydraulic continuity requirements between the blocks. The solution is used to predict the spatial drawdown distribution in a wide variety of anticline aquifer system and to investigate the influences of well location, screen length, aquifer geometry and anisotropy on the flow system. Moreover, the present solution is applied to simulate the flow in hillslope and slab-shaped aquifers by assuming some of the adjacent blocks with the same heights. In addition to the analytical approach, the numerical model, MODFLOW, is used to perform simulations and the results are compared with those predicted by the present solution. The solution can also be employed to estimate the aquifer parameters in an inverse problem if integrated with an optimization algorithm.

CHAPTER 2 METHODOLOGY

2.1 Mathematical modeling of the flow problem

Figure 1 shows the configuration for a well in an anticline aquifer. We assume that the line sink, i.e., the pumping well of an infinitesimal radius, is extended along the z direction with length l from the point $(x_0, y_0, z_0) = (0, 0, z_0)$. The anticline aquifer has a finite width in the x direction, a finite thickness in the z direction, but infinite extent in both $\pm y$ directions. In addition, the aquifer is confined, homogeneous, and anisotropic with the hydraulic conductivities of k_x , k_y and k_z respectively in the x , y and z directions. To simplify the flow problem, three successive blocks with different height and width are used to mimic the topographical shape of anticline aquifer as shown in Figure 1. The height of the middle block is determined by the acme of the anticline structure while those of the adjacent blocks are designated by the corresponding margins of the limbs. The adopted widths of the blocks should make the approximated aquifer has the same volume as the original one as possible. Furthermore, the anticline aquifer is decomposed into four subdomains, i.e., zones 1P, 1N, 2 and 3, according to the shapes of blocks and the well location.

The mathematical model is developed in a dimensionless form to produce the simulated results in the most general way. The height of the middle block, b_1 , is

chosen as a reference length to nondimensionalize other variables. The dimensionless variables and parameters are defined as follows: $x_D = x/b_1$, $y_D = y/b_1$, and $z_D = z/b_1$ denoting the dimensionless coordinate variables; $x_{0D} = x_0/b_1$, $y_{0D} = y_0/b_1$, and $z_{0D} = z_0/b_1$ representing the top point of the pumping well in the dimensionless form; $x_{Dai} = a_i/b_1$ representing the dimensionless distance in x -direction of the outer boundary from the origin in zone i ; $z_{Dbi} = b_i/b_1$ defining the dimensionless height of zone i , except that $z_{Db1} = 1$ standing for those in zones 1P and 1N; $s_{Di} = s_i/b_1$ denoting the dimensionless drawdown in zone i , where the notation s_i is the drawdown in zone i (L); $z_{Dl} = l/b_1$ representing the dimensionless screen length of the pumping well; $q_D = q/k_x b_1$ expressing the dimensionless volumetric pumping rate per unit length of the pumping well, where the notation q is the volumetric pumping rate per unit length ($L^2 T^{-1}$); $\chi_{yx} = k_y/k_x$ and $\chi_{zx} = k_z/k_x$ representing the anisotropy ratios.

2.1.1 Formulation for flow in zone 1

In the construction of the mathematical model, the middle block (shown in Figure 1) is regarded as zone 1, which includes zones 1P and 1N. The steady-state groundwater flow to the pumping well in zone 1 is governed by

$$\frac{\partial^2 s_{D1}}{\partial x_D^2} + \chi_{yx} \frac{\partial^2 s_{D1}}{\partial y_D^2} + \chi_{zx} \frac{\partial^2 s_{D1}}{\partial z_D^2} = -q_D \{ U[z_D - (z_{0D} - z_{D1})] - U(z_D - z_{0D}) \} \delta(x_D - x_{0D}) \delta(y_D - y_{0D}),$$

$$x_{Da1N} \leq x_D \leq x_{Da1P}, \quad -\infty \leq y_D \leq \infty, \quad 0 \leq z_D \leq 1 \quad (1)$$

where U and δ are the unit step function and Dirac delta function, respectively.

The sink term in Eq. (1) implies that the flux through the screen is of uniform strength.

The boundary conditions at infinity from the sink in the y direction are assumed to

be

$$s_{D1}(x_D, \pm\infty, z_D) = 0 \quad (2)$$

and

$$\frac{\partial s_{D1}(x_D, \pm\infty, z_D)}{\partial y_D} = 0 \quad (3)$$

For a confined aquifer, the conditions at the top and bottom impermeable boundaries are respectively written as

$$\frac{\partial s_{D1}(x_D, y_D, 1)}{\partial z_D} = 0 \quad (4)$$

and

$$\frac{\partial s_{D1}(x_D, y_D, 0)}{\partial z_D} = 0 \quad (5)$$

The continuities of flux and drawdown at the right-hand edge of zone 1 are

respectively as

$$\frac{\partial s_{D1}(x_{Da1P}, y_D, z_D)}{\partial x_D} = \begin{cases} \frac{\partial s_{D2}(x_{Da1P}, y_D, z_D)}{\partial x_D}, & 0 \leq z_D < z_{Db2} \\ 0, & z_{Db2} \leq z_D \leq 1 \end{cases} \quad (6a)$$

$$(6b)$$

and

$$s_{D1}(x_{Da1P}, y_D, z_D) = s_{D2}(x_{Da1P}, y_D, z_D), \quad 0 \leq z_D < z_{Db2} \quad (7)$$

Similarly, for the left-hand edge of zone 1, the following conditions should be satisfied:

$$\frac{\partial s_{D1}(x_{Da1N}, y_D, z_D)}{\partial x_D} = \begin{cases} \frac{\partial s_{D3}(x_{Da1N}, y_D, z_D)}{\partial x_D}, & 0 \leq z_D < z_{Db3} \\ 0, & z_{Db3} \leq z_D \leq 1 \end{cases} \quad (8a)$$

$$(8b)$$

and

$$s_{D1}(x_{Da1N}, y_D, z_D) = s_{D3}(x_{Da1N}, y_D, z_D), \quad 0 \leq z_D < z_{Db3} \quad (9)$$

2.1.2 Formulation for flow in zone 2

The steady-state groundwater flow equation in zone 2 is expressed as:

$$\frac{\partial^2 s_{D2}}{\partial x_D^2} + \chi_{yx} \frac{\partial^2 s_{D2}}{\partial y_D^2} + \chi_{zx} \frac{\partial^2 s_{D2}}{\partial z_D^2} = 0, \quad x_{Da1P} \leq x_D \leq x_{Da2}, \quad -\infty \leq y_D \leq \infty, \quad 0 \leq z_D \leq z_{Db2} \quad (10)$$

The boundary conditions at infinity in the $\pm y$ directions require that

$$s_{D2}(x_D, \pm \infty, z_D) = 0 \quad (11)$$

and

$$\frac{\partial s_{D2}(x_D, \pm \infty, z_D)}{\partial y_D} = 0 \quad (12)$$

The no-flow conditions hold at the top and bottom boundaries respectively as

$$\frac{\partial s_{D2}(x_D, y_D, z_{Db2})}{\partial z_D} = 0 \quad (13)$$

and

$$\frac{\partial s_{D2}(x_D, y_D, 0)}{\partial z_D} = 0 \quad (14)$$

Assume that a constant-head boundary located at the lateral distance of x_{Da2} from the pumping well; that is,

$$s_{D2}(x_{Da2}, y_D, z_D) = 0 \quad (15)$$

Note that Eqs. (6a) and (7), representing the continuity conditions of flux and drawdown at the interface between zones 1P and 2, are the left-hand boundary conditions of zone 2.

2.1.3 Formulation for flow in zone 3

The steady-state groundwater flow equation in zone 3 is given by

$$\frac{\partial^2 s_{D3}}{\partial x_D^2} + \chi_{yx} \frac{\partial^2 s_{D3}}{\partial y_D^2} + \chi_{zx} \frac{\partial^2 s_{D3}}{\partial z_D^2} = 0, \quad x_{Da3} \leq x_D \leq x_{Da1N}, \quad -\infty \leq y_D \leq \infty, \quad 0 \leq z_D \leq z_{Db3} \quad (16)$$

The boundary conditions at infinite distance in the $\pm y$ directions require that

$$s_{D3}(x_D, \pm \infty, z_D) = 0 \quad (17)$$

and

$$\frac{\partial s_{D3}(x_D, \pm \infty, z_D)}{\partial y_D} = 0 \quad (18)$$

The top and bottom conditions in zone 3 are respectively given as

$$\frac{\partial s_{D3}(x_D, y_D, z_{Db3})}{\partial z_D} = 0 \quad (19)$$

and

$$\frac{\partial s_{D3}(x_D, y_D, 0)}{\partial z_D} = 0 \quad (20)$$

A constant-head condition is applied at the lateral distance of x_{Da3} from the pumping well, which is described as

$$s_{D3}(x_{Da3}, y_D, z_D) = 0 \quad (21)$$

Furthermore, Eqs. (8a) and (9) state the continuity requirements of flux and drawdown at the interface between zones 1N and 3.

2.2 Analytical solutions

2.2.1 Dimensionless drawdown solutions for zones 2 and 3

To solve the partial differential equations (1), (10), and (16) with their corresponding boundary conditions, the techniques of FT and FFCT are used with respect to the variables y_D and z_D , respectively, to obtain the ordinary differential equations (ODEs) in terms of x_D . Note that formulas of FFCT applied to (1), (10), and (16) are different since the independent variable z_D ranges over different intervals in zones 1, 2, and 3, respectively. We first deal with the flow problem in zones 2 and 3 since their governing equations are simple and of the same form. The integral transforms and derivations for the solutions are given in Appendix A. The dimensionless drawdown solution of zone 2 in Fourier domain satisfying the conditions (10) to (15) is given as:

$$\bar{s}_{D2}(x_D, z_D) = V_0 A_0(x_D) + \sum_{n=1}^{\infty} V_n A_n(x_D) \cos(\omega_n z_D) \quad (22)$$

where

$$A_n(x_D) = \frac{\sinh[\alpha_n(x_{Da2} - x_D)]}{\sinh[\alpha_n(x_{Da2} - x_{Da1P})]}, \quad n = 0, 1, 2, 3, \dots \quad (23)$$

with

$$\alpha_n = \sqrt{\varepsilon^2 \chi_{yx} + \omega_n^2 \chi_{zx}}, \quad n = 0, 1, 2, 3, \dots \quad (24)$$

In Eq. (24), ε is the FT transform variable; ω_n is the transform variable used with respect to Eq. (10) in the FFCT for the integral interval $[0, z_{Db2}]$, which is defined as

$$\omega_n = \frac{n\pi}{z_{Db2}}, \quad n = 0, 1, 2, 3, \dots \quad (25)$$

Note that the coefficients V_0 and V_n are the constants needed to be determined by

the remaining boundary conditions (6a) and (7).

As for zone 3, the dimensionless drawdown solution of Eq. (16) in Fourier domain satisfying conditions (17) to (21) is expressed in the series form as:

$$\bar{s}_{D3}(x_D, z_D) = W_0 B_0(x_D) + \sum_{k=1}^{\infty} W_k B_k(x_D) \cos(\zeta_k z_D) \quad (26)$$

where

$$B_k(x_D) = \frac{\sinh[\beta_k(x_{Da3} - x_D)]}{\sinh[\beta_k(x_{Da3} - x_{Da1N})]}, \quad k = 0, 1, 2, 3, \dots \quad (27)$$

with

$$\beta_k = \sqrt{\varepsilon^2 \chi_{yx} + \zeta_k^2 \chi_{zx}}, \quad k = 0, 1, 2, 3, \dots \quad (28)$$

and ζ_k being the transform variable used in the FFCT to Eq. (16) for the integral

interval $[0, z_{Db3}]$, which is defined as

$$\zeta_k = \frac{k\pi}{z_{Db3}}, \quad k = 0, 1, 2, 3, \dots \quad (29)$$

The coefficients W_0 and W_k in Eq. (26) are the remaining undetermined constants.

2.2.2 Dimensionless drawdown solution for zone 1

The presence of line sink term in Eq. (1) makes it complicated to derive the solution. First, the FT with respect to y_D and FFCT with respect to z_D are applied to Eq. (1) and the result is

$$\frac{d^2 \hat{s}_{D1}}{dx_D^2} - (\varepsilon^2 \chi_{yx} + \lambda_m^2 \chi_{zx}) \hat{s}_{D1} = -q_D U_c \delta(x_D - x_{0D}), \quad x_{Da1N} \leq x_D \leq x_{Da1P} \quad (30)$$

where \hat{s}_{D1} is the dimensionless drawdown in Fourier and Finite Fourier cosine domain; λ_m is the transform variable used in the FFCT to Eq. (1) for the integral interval $[0, 1]$, which is defined as

$$\lambda_m = m\pi, \quad m = 0, 1, 2, 3, \dots \quad (31)$$

In addition,

$$U_c = \int_{z_{0D} - z_{Dl}}^{z_{0D}} \cos(\lambda_m z_D) dz_D \quad (32)$$

which can be reduced to $U_c = U_{c0} = z_{Dl}$ when $m = 0$; otherwise,

$$U_c = U_{cm} = \frac{\sin(\lambda_m z_{0D}) - \sin[\lambda_m (z_{0D} - z_{Dl})]}{\lambda_m}, \quad m = 1, 2, 3, \dots \quad (33)$$

To solve Eq. (30) with the term of Dirac delta function, we consider the following sets

of ODEs by dividing zone 1 into zones 1P and 1N as:

$$\frac{d^2 \hat{s}_{D1P}}{dx_D^2} - (\varepsilon^2 \chi_{yx} + \lambda_m^2 \chi_{zx}) \hat{s}_{D1P} = 0, \quad 0 < x_D \leq x_{Da1P} \quad (34)$$

and

$$\frac{d^2 \hat{s}_{D1N}}{dx_D^2} - (\varepsilon^2 \chi_{yx} + \lambda_m^2 \chi_{zx}) \hat{s}_{D1N} = 0, \quad x_{Da1N} \leq x_D < 0 \quad (35)$$

The boundary condition at $x_D = 0$ due to the continuity must be satisfied, which is expressed as

$$\hat{s}_{D1P}(0^+) = \hat{s}_{D1N}(0^-) \quad (36)$$

Integration of (30) with respect to x_D along 0^- to 0^+ yields the second boundary condition as

$$\frac{d\hat{s}_{D1P}(0^+)}{dx_D} - \frac{d\hat{s}_{D1N}(0^-)}{dx_D} = -q_D U_c \quad (37)$$

The dimensionless drawdown solutions for zones 1P and 1N in Fourier domain can be obtained by taking the inversion of FFCT to the solutions of (34) and (35) with conditions (36) and (37). Applying Eqs. (6) and (8) to the solutions of zones 1P and 1N, respectively, yields

$$\begin{aligned} \bar{s}_{D1P}(x_D, z_D) = & \frac{q_D U_{c0}}{2\gamma_0} [C_{10}(x_D) + C_{20}(x_D)] - z_{Db2} C_{30} C_{40}(x_D) V_0 + z_{Db3} C_{50} C_{60}(x_D) W_0 \\ & + \sum_{m=1}^{\infty} \left\{ \begin{aligned} & \frac{q_D U_{cm}}{\gamma_m} [C_{1m}(x_D) + C_{2m}(x_D)] \\ & - \frac{2}{\gamma_m} \left\{ \left[\frac{\sin(\lambda_m z_{Db2})}{\lambda_m} \right] \alpha_0 C_{30} V_0 + \sum_{n=1}^{\infty} \phi(m, n) \alpha_n C_{3n} V_n \right\} C_{4m}(x_D) \\ & + \frac{2}{\gamma_m} \left\{ \left[\frac{\sin(\lambda_m z_{Db3})}{\lambda_m} \right] \beta_0 C_{50} W_0 + \sum_{k=1}^{\infty} \vartheta(m, k) \beta_k C_{5k} W_k \right\} C_{6m}(x_D) \end{aligned} \right\} \cos(\lambda_m z_D) \end{aligned} \quad (38)$$

for describing the dimensionless drawdown in zone 1P and

$$\bar{s}_{D1N}(x_D, z_D) = \frac{q_D U_{c0}}{2\gamma_0} [C_{10}(x_D) + C_{70}(x_D)] - z_{Db2} C_{30} C_{40}(x_D) V_0 + z_{Db3} C_{50} C_{60}(x_D) W_0$$

$$+ \sum_{m=1}^{\infty} \left\{ \begin{array}{l} \frac{q_D U_{cm}}{\gamma_m} [C_{1m}(x_D) + C_{7m}(x_D)] \\ - \frac{2}{\gamma_m} \left\{ \left[\frac{\sin(\lambda_m z_{Db2})}{\lambda_m} \right] \alpha_0 C_{30} V_0 + \sum_{n=1}^{\infty} \phi(m, n) \alpha_n C_{3n} V_n \right\} C_{4m}(x_D) \\ + \frac{2}{\gamma_m} \left\{ \left[\frac{\sin(\lambda_m z_{Db3})}{\lambda_m} \right] \beta_0 C_{50} W_0 + \sum_{k=1}^{\infty} \vartheta(m, k) \beta_k C_{5k} W_k \right\} C_{6m}(x_D) \end{array} \right\} \cos(\lambda_m z_D)$$
(39)

for describing the dimensionless drawdown in zone 1N, where

$$\gamma_m = \sqrt{\varepsilon^2 \chi_{yx} + \lambda_m^2 \chi_{zx}}, \quad m = 0, 1, 2, 3, \dots \quad (40)$$

$$C_{1m}(x_D) = \frac{\cosh[\gamma_m (x_{Da1P} + x_{Da1N} - x_D)]}{\sinh[\gamma_m (x_{Da1P} - x_{Da1N})]}, \quad m = 0, 1, 2, 3, \dots \quad (41)$$

$$C_{2m}(x_D) = \frac{\cosh[\gamma_m (x_{Da1P} - x_{Da1N} - x_D)]}{\sinh[\gamma_m (x_{Da1P} - x_{Da1N})]}, \quad m = 0, 1, 2, 3, \dots \quad (42)$$

$$C_{3n} = \coth[\alpha_n (x_{Da2} - x_{Da1P})], \quad n = 0, 1, 2, 3, \dots \quad (43)$$

$$C_{4m}(x_D) = \frac{\cosh[\gamma_m (x_{Da1N} - x_D)]}{\sinh[\gamma_m (x_{Da1P} - x_{Da1N})]}, \quad m = 0, 1, 2, 3, \dots \quad (44)$$

$$C_{5k} = \coth[\beta_k (x_{Da3} - x_{Da1N})], \quad k = 0, 1, 2, 3, \dots \quad (45)$$

$$C_{6m}(x_D) = \frac{\cosh[\gamma_m (x_{Da1P} - x_D)]}{\sinh[\gamma_m (x_{Da1P} - x_{Da1N})]}, \quad m = 0, 1, 2, 3, \dots \quad (46)$$

$$C_{7m}(x_D) = \frac{\cosh[\gamma_m (x_{Da1P} - x_{Da1N} + x_D)]}{\sinh[\gamma_m (x_{Da1P} - x_{Da1N})]}, \quad m = 0, 1, 2, 3, \dots \quad (47)$$

$$\phi(m, n) = \begin{cases} \frac{\sin[(\lambda_m + \omega_n) z_{Db2}]}{2(\lambda_m + \omega_n)} + \frac{z_{Db2}}{2}, & \text{for } \lambda_m = \omega_n \end{cases} \quad (48a)$$

$$\left\{ \frac{\sin[(\lambda_m + \omega_n) z_{Db2}]}{2(\lambda_m + \omega_n)} + \frac{\sin[(\lambda_m - \omega_n) z_{Db2}]}{2(\lambda_m - \omega_n)} \right\}, \quad \text{for } \lambda_m \neq \omega_n \quad (48b)$$

and

$$\vartheta(m, k) = \begin{cases} \frac{\sin[(\lambda_m + \zeta_k) z_{Db3}]}{2(\lambda_m + \zeta_k)} + \frac{z_{Db3}}{2}, & \text{for } \lambda_m = \zeta_k \end{cases} \quad (49a)$$

$$\left\{ \frac{\sin[(\lambda_m + \zeta_k) z_{Db3}]}{2(\lambda_m + \zeta_k)} + \frac{\sin[(\lambda_m - \zeta_k) z_{Db3}]}{2(\lambda_m - \zeta_k)} \right\}, \quad \text{for } \lambda_m \neq \zeta_k \quad (49b)$$

Substituting Eqs. (22) and (38) into Eq. (7), the coefficients V_0 and V_n can be expressed as the functions of V_0 , V_n , W_0 and W_k via the determination of the coefficients in the Fourier cosine series. Similarly, the coefficients W_0 and W_k are related to V_0 , V_n , W_0 and W_k by the Fourier cosine series of substituting (26) and (39) into (9). The coefficients V_0 , V_n , W_0 and W_k can then be solved in the matrix form as presented in Appendix B (i.e., Eq. (B1)).

2.3 Numerical Evaluations

2.3.1 Calculation on Eqs. (22), (26), (38), and (39)

In this study, all of the numerical evaluations are made via FORTRAN with double precision. The drawdown solutions given by Eqs. (22), (26), (38), and (39) require the evaluation of infinite series with the coefficients V_0 , V_n , W_0 and W_k determined by Eq. (B1). The subroutine DLSLRG of IMSL (2003) is used to solve Eq. (B1) by setting $i = j = k = n$ up to 100; accordingly, 202 linear equations should be solved simultaneously. In addition, the Shanks' transform method (Shanks, 1955) as a technique of accelerating the convergence of sequences is applied to compute the summation within 100 terms.

2.3.2 Inverse Fourier Transform

The FT of function $f(y_D)$ with respect to the variable y_D is defined as (Jaffrey and Dai, 2008):

$$\bar{f}(\varepsilon) = \int_{-\infty}^{\infty} f(y_D) e^{-i\varepsilon y_D} dy_D \quad (50)$$

where $\bar{f}(\varepsilon)$ is the transformed function and its inversion is expressed as

$$f(y_D) = \frac{1}{2\pi} \int_{-\infty}^{\infty} \bar{f}(\varepsilon) e^{i\varepsilon y_D} d\varepsilon \quad (51)$$

The function $\bar{f}(\varepsilon)$ can refer to the drawdown solutions, Eqs. (22), (26), (38), and (39), in the Fourier domain for the flow in the anticline aquifer. Since the drawdown

solutions are even functions with respect to the variable ε , Eq. (51) can be reduced to

$$f(y_D) = \frac{1}{\pi} \int_0^{\infty} \bar{f}(\varepsilon) \cos(\varepsilon y_D) d\varepsilon \quad (52)$$

The numerical evaluation of Eq. (52) is achieved by the routine DQDAWF of IMSL (2003), which has the ability to cope with integrals of semi-infinite interval and of cosine or sine integrands.

2.4 Numerical Simulations in MODFLOW

MODFLOW (McDonald and Harbaugh, 1988; Harbaugh and McDonald, 1996a, 1996b) is a computer program, developed based on the block-centered finite difference method, that simulates the three-dimensional groundwater flow in a porous

medium. The heads in each cell are calculated by solving the finite-difference flow equations for the head at a node and its six adjacent nodes at the end of a time step. The equations for the entire grid are expressed in a matrix form and solved simultaneously at each time step. In this study, we use the software Processing MODFLOW for Windows (PMWIN) version 5.3 (Chiang and Kinzelbach, 2001), which provides a graphical interface and integrated platform for the program, to simulate the flow in a groundwater system. The users can easily prepare the grid information and the related input data, e.g., initial condition, boundary conditions, and hydrogeological parameters, via PMWIN for the problem. The grid discretization and other setting information corresponding to the simulated cases will be demonstrated thereafter. The preconditioned conjugate-gradient package 2 (PCG2 package) is chosen to solve the equation system. The iteration stops when the maximum number of iterations are achieved or absolute value of the head change and the residual of the matrix at all nodes during an iteration are less than or equal to 0.001 m and 0.001 m³/s, respectively. The outer iterations update the coefficient matrix and the vector, which is associated with head-dependent boundary conditions at each cell, in the equation system with the newly calculated hydraulic heads. The inner iterations solve the new set of coefficient matrix and vector. The maximum numbers of outer and inner iterations are setting as 50 and 30, respectively.

CHAPTER 3 RESULTS AND DISCUSSION

3.1 Special cases

3.1.1 Slab-shaped aquifer bounded by parallel constant-head boundaries

The present solution can be simplified to describe the pumping in an isotropic slab-shaped aquifer bounded by two parallel constant-head boundaries along y-direction if the three blocks are of the same height, i.e., $z_{Db1} = z_{Db2} = z_{Db3} = 1$. In this section, we assume a fully penetrating well pumped at a dimensionless flow rate of $Q_D = q_D z_{Di} = 1$ and located at the middle of the slab-shaped aquifer with $x_{Da2} = 1$ and $x_{Da3} = -1$. Accordingly, no vertical flow appears in the aquifer, i.e., the dimensionless drawdown solution is not a function of z_D . The same problem can refer to Ferris et al. (1962, Figure 42), who illustrates the application of image-well method for the pumping in an aquifer bounded by two parallel boundaries. The solution for drawdown at an observation well can be evaluated as the sum of the drawdowns and buildups due to the pumping well and image wells. If an observation well is located at the dimensionless distance of r_D from the pumping well, the dimensionless drawdown at the well can be formulated by superposition of Theis solution (1935) as

$$s_D(r_D, t_D) = \frac{Q_D}{4\pi} \left[W(u_p) + \sum_{m=1}^{\infty} (-1)^m W(u_{im}) + \sum_{n=1}^{\infty} (-1)^n W(u_{in}) \right] \quad (53)$$

where W is the well function; u_p , u_{im} , and u_{in} are the dimensionless variables

respectively defined as

$$u_p = \frac{r_D^2}{4t_D} \quad (54)$$

$$u_{im} = \frac{r_D^2 + 4m^2 - 4mr_D \cos \theta}{4t_D} \quad (55)$$

and

$$u_{in} = \frac{r_D^2 + 4n^2 - 4nr_D \cos(\pi - \theta)}{4t_D} \quad (56)$$

in which θ is the angle between the positive x_D -axis and the line connecting the pumping and observation wells; t_D is the dimensionless time defined as

$$t_D = \frac{Tt}{b_1^2 S} \quad (57)$$

with T and S are the transmissivity and storativity of the aquifer, respectively.

Note that t_D should be large enough and the flow system reaches the steady state so

that the dimensionless drawdowns calculated by the image-well method and the simplified solution can be compared. The value of the infinite series in Eq. (53) is

evaluated by the Shanks method (1955) to accelerate the convergence. Figure 2

compares the dimensionless drawdown calculated by the present solution and Eq. (53)

for pumping at the middle of the slab-shaped aquifer bounded by two parallel

constant-head boundaries. The dimensionless drawdown are calculated along the

radial direction when $\theta = 0$, $\pi/4$, and $\pi/2$. The dimensionless drawdown

distributions predicted by the present solution in this special case match very well

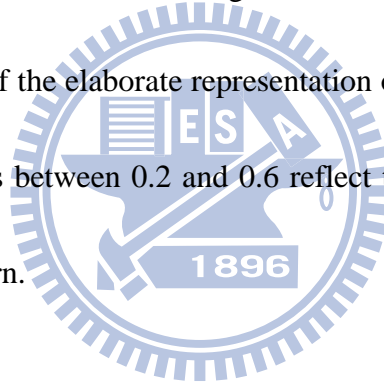
with those predicted by Eq. (53).

3.1.2 Hillslope aquifer

The simulation for flow in a hillslope confined aquifer due to pumping is carried out by setting two of the adjacent blocks with the same height. Assume a hillslope aquifer is mimicked by the step-like aquifer, which has $x_{Da1P} = 0.5$, $x_{Da1N} = -0.5$, $x_{Da2} = 2$, $x_{Da3} = -1$, $z_{Db1} = z_{Db3} = 1$, and $z_{Db2} = 0.5$ with a fully penetrating well pumped at a dimensionless pumping rate of $Q_D = 1$. Figure 3a shows that at steady state the contour lines of the dimensionless drawdown and the flow field are influenced by the inclination in the hillslope aquifer. The vertical flow appears around the concave corner of the top boundary while the flow seems horizontal elsewhere.

The simulation results for the hillslope aquifer from MODFLOW are compared with that evaluated by the present solution. The confined aquifer simulated by MODFLOW is bounded by two parallel constant-head boundaries with the distance of 30 m in width. The aquifer thickness varies from 10 m to 5 m in the hillslope. Note that the infinite boundaries in the \pm y-directions are replaced by assigning two constant-head boundaries located at ± 40 m from the pumping well. The hydraulic conductivities are 10^{-4} m/s in the x-, y- and z-directions. The pumping rate at the well is 10^{-2} m³/s so that the dimensionless pumping rate will be $Q_D = 1$. The length of time is set to be 9.46728×10^7 s (1095.75 day) for the steady-state simulation.

The model domain has been discretized using a uniform cubic grid with a step of 0.5 m. That is, the aquifer is discretized with 21 layers, 61 columns, and 161 rows. Figure 3b provides simulated results in the dimensionless form using MODFLOW for the case that the hillslope aquifer is mimicked by the step-like aquifer, as that used in Figure 3a. The figure indicates slight difference on the drawdown distribution occurs near the concave corner of the top boundary, taking the dimensionless drawdown contour of 0.3 for comparison, between the present solution and MODFLOW. The flow pattern shown in Figure 3c is a more reasonable one among those in Figure 3 because of the elaborate representation on the slope boundary. The significant flexure contours between 0.2 and 0.6 reflect the influence of top inclined boundary on the flow pattern.



3.2 Base case of anticline aquifer

To investigate the influence of aquifer geometry on the flow pattern, we assume a simple case of a fully penetrating well located at an isotropic anticline aquifer. Figure 4a depicts the dimensionless drawdown in the $x_D - z_D$ plane for $y_D = 0$ when the constant-flux pumping at the anticline aquifer with the geometry $x_{Da1P} = 0.5$, $x_{Da1N} = -0.5$, $x_{Da2} = 1$, $x_{Da3} = -1$, and $z_{Db2} = z_{Db3} = 0.5$. The well pumps at a dimensionless flow rate of $Q_D = 1$. The dimensionless drawdown contours reveal

that most of water flows horizontally around the well screen and in the limbs; however, conspicuous vertical flow appears around the concave corner of the top boundary. Figures 4b and 4c show the drawdown distribution in the $y_D - z_D$ plane for $x_D = 0.2$ and 0.8 , respectively. The value of y_D ranges from 0 to 1 since the dimensionless drawdown distribution is expected to be symmetrical with respect to the plane $y_D = 0$ and little concern may be paid on the drawdown distribution that is far away from the well. The dimensionless drawdown contours intersect with the top and bottom impervious boundaries at right angles. The figures indicate that the anisotropy of the aquifer indeed affects the three-dimensional flow pattern; otherwise, the contours in Figure 4 should be parallel to the z_D -axis for the case with a fully penetrating well. At steady state, water flow to a well in the system comes from two sources: the constant-head boundaries at $x_D = \pm 1$ and the remote boundaries in the y -direction. However, in the upper part of the ridge zone, there are limited flows from the former source due to the anisotropy of the aquifer. Therefore, as shown in Figures 4b and 4c, the dimensionless drawdown increases with z_D at a given x_D and y_D to sustain the uniform and constant-flux condition along the whole well screen. This fact also implies the presence of the vertical upward flow, especially near $y_D = 0$.

Figure 5 illustrates the dimensionless drawdown contours being predicted by

MODFLOW for the case of identical well and aquifer system as Figure 4. In the simulation, the anticline aquifer is bounded by two parallel constant-head boundaries with a distance of 20 m in width. The acme of the anticline structure is 10 m in height; the limbs intersect with the two parallel constant-head boundaries at 5 m in height. The settings of the y-direction boundaries, hydraulic conductivities, pumping rate and time length are the same as those used in the simulation of the hillslope aquifer. The aquifer is discretized into a mesh with 21 layers, 41 columns and 161 rows. The drawdown contours in Figure 5a seem similar to those depicted in Figure 4a except that slight differences can be observed around the concave corner of the top boundary and the pumping well. In adjacent to the pumping well, MODFLOW gives smaller dimensionless drawdown than the present solution. Figures 5b and 5c show the simulated results based on MODFLOW for the dimensionless drawdown contours in the $y_D - z_D$ plane for $x_D = 0.2$ and 0.8, respectively. On the top-left region of both figures, the dimensionless drawdown values calculated by MODFLOW are small in comparison with those evaluated by the present solution as illustrated in Figures 4b and 4c.

Figure 6 shows the dimensionless drawdown contours predicted by the MODFLOW for the flow in the anticline aquifer with the top curved boundary being mimicked by multiple steps. The settings of the x-direction and y-direction

boundaries, hydraulic conductivities, pumping rate and time length are the same as those used in the simulation of Figure 5. The aquifer is discretized into a mesh with 21 layers, 41 columns and 161 rows. Figure 6a shows that the flow to a fully penetrating well in an anticline aquifer with its top boundary being mimicked by multiple steps results in the smooth and curved drawdown contours in the profile. Figures 6b and 6c exhibit the dimensionless drawdown contours in the $y_D - z_D$ plane for $x_D = 0.2$ and 0.8 , respectively. The dimensionless drawdown values plotted in Figures 6a and 6b are smaller than those in Figures 5a and 5b, respectively. The oblique contours shown in Figure 6c imply that there is much more vertical flow occurs on this profile; additionally, the predicted drawdown values are significantly smaller in the bottom region (around $0 < z_D < 0.4$) and larger near the top region (around $0.4 < z_D < 0.5$) when comparing with the contours sketched in Figures 5c for the region $0 < z_D < 0.5$. Moreover, the contours intersected with the top boundaries at bevel angles, especially in Figure 6c, due to the coarse discretization on the model grid. Comparing the results sketched in Figures 5 and 6 indicate that one may overestimate the dimensionless drawdown when applying the simple one-step like top boundary to simulate the anticlinal geometry.

3.3 Effect of anticline aquifer geometry

Figure 7 examines two other aquifers with different geometries by considering the aquifer portrayed in Figure 4 as a base case. For an anticline aquifer of thin limbs, as shown in Figure 7a, the height of the limbs are reduced to half of that in the base case, i.e., $z_{Db2} = z_{Db3} = 0.25$. In addition, Figure 7b depicts the case of narrow-ridged anticline with $x_{Da1P} = 0.25$ and $x_{Da1N} = -0.25$. Similar to the results of the base case, both figures show that most of water flows horizontally in the zone around the well and in the limbs. Significant vertical flow appears around the concave corner of the top boundary in the ridge zone due to the geometric variation. The anticline aquifers with thin limbs or narrow ridge both cause a sharp head drop in the ridge zone in comparison with that of the base case at steady state. Figure 8 compares the dimensionless drawdown distribution along $(y_D, z_D) = (0, 1)$ for these two cases with that of the base case. The figure again indicates that the cases of thin limbs and narrow ridge both have much larger head drop at steady state than that of the base case.

3.4 Effect of well partial penetration

3.4.1 Effect of screen length and aquifer anisotropy

Figure 9 demonstrates the largest dimensionless drawdown at

$(x_D, y_D) = (0.001, 0)$ along the z-direction for the cases of different dimensionless screen length of $z_{Dl} = 0.2, 0.4, 0.6, 0.8$ and 1.0 and various aquifer anisotropy ratios of $\chi_{zx} = 0.3, 1.0,$ and 3.0 . The wells are screened from the top of the aquifer with a constant dimensionless pumping rate of $Q_D = 1$. Among these cases, the largest dimensionless drawdown appears at the case of the smallest χ_{zx} and z_{Dl} ($\chi_{zx} = 0.3$ and $z_{Dl} = 0.2$) near the top of the aquifer. Moreover, the influence of aquifer anisotropy on the drawdown increases with the decrease of screen length.

Figures 10a and 10b display the dimensionless drawdown contours for the anisotropic cases of $\chi_{zx} = 0.3$ and 3 , respectively. In Figure 10a, significant vertical flow can be observed in the ridge and limb zones. The contours for $s_D = 0.3$ to 0.8 are nearly horizontal, which reflect apparent vertical flow cross this region. Because of k_x is larger than k_z in this case ($\chi_{zx} = 0.3$), most of flow goes through the horizontal path surrounding the well leading to the larger drawdown in the upper zone 1 (i.e., $0.8 \leq z_D < 1$). The resultant hydraulic gradient as well as the boundary restriction causes an obvious vertical flow below this zone. On the other hand, Figure 10b represents an uncommon case of k_z being larger than k_x ($\chi_{zx} = 3$). In this case, the vertical path for flow into the well is superior to the horizontal one, which results in the contours around the well look like half ellipses. The flow in the limbs is mainly horizontal. However, obviously vertical flow can be observed in the

central zone 1 below the well ($z_D < 0.8$ and $|x_D| < 0.2$) and around the concave corner of the top boundary in the anticline.

3.4.2 Effect of penetration ratio

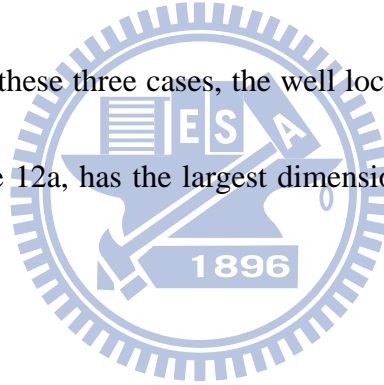
The penetration ratio, i.e., the ratio of well screen length to aquifer thickness, in the real anticline aquifer and approximated aquifer may be different if the partially penetrating well is not located at the $y_D - z_D$ plane that contains the acme of anticline and used to determine the height of zone 1. Considering the case of an anticline aquifer whose top boundary consists of isosceles ramps, the simulation of drawdown distribution is achieved based on the present solution via approximating the aquifer geometry as the base case. A partially penetrating well with the dimensionless screen length of 0.8 is located at a dimensionless x_D distance of 0.25 from the midline of the anticline aquifer, where the real dimensionless thickness of aquifer would be 0.875. Therefore, the penetration ratio is 0.914 for the well in the real anticline aquifer. Note that the ratio, however, becomes 0.8 in the approximated aquifer if the dimensionless screen length in the simulation maintains the same as the real one. To investigate the effect of distorted penetration ratio applied in the simulation, Figure 11 shows the drawdown distributions for three partially penetrating wells with z_{Dl} being equal to 0.8, 0.857, and 0.914. In the simulation, the cases of

$z_{Dl} = 0.8$ and 0.914 represent the use of real dimensionless screen length and dimensionless screen length in the approximated aquifer that has the penetration ratio the same as that in the real aquifer, respectively. Furthermore, the case of $z_{Dl} = 0.857$ represents the average between two aforementioned lengths. In Figure 11, the dimensionless drawdown contours for the flow to the three partially penetrating wells differ considerably at the top region of ridge zone and around the top end of the well. However, the use of $z_{Dl} = 0.8$ would be the better one to simulate the flow toward the top end of the well.

3.4.3 Effect of well location

Figure 12 illustrates the influence of well location on the flow pattern. The dimensionless screen length of the partially penetrating well is considered to be $z_{Dl} = 0.2$; additionally, the isotropic anticline aquifer has the same geometry as the base case. Figures 12a and 12b display the dimensionless drawdown contours at $y_D = 0$ for the pumping at a partially penetrating well located at the top-middle and bottom-middle of the aquifer, respectively. The flow patterns on the profile are symmetrical to the midline of the aquifer. Most of water flows horizontally in the limbs except in the zone near the concave corner of the top boundary. Obviously upward and downward vertical flows occur in the aquifer as illustrated in Figures 12a

and 12b, respectively, especially in the zone toward the extremity of the well. The present solution can simulate the dimensionless drawdown for an arbitrarily located pumping well in the ridge zone. In the case of Figure 12c, the partially penetrating well with the dimensionless screen length of 0.2 is located at a dimensionless distance of 0.25 from the midline of the anticline aquifer. Also note that the geometry of anticline aquifer in Figure 12c is the same as that in the base case. The figure shows an asymmetrical flow pattern affected by the well location and aquifer geometry. Considerable vertical flow appears in the ridge zone and in the right limb where $x_D < 0.35$. In addition, among these three cases, the well located at the top-middle of the aquifer, as shown in Figure 12a, has the largest dimensionless drawdown around the well.



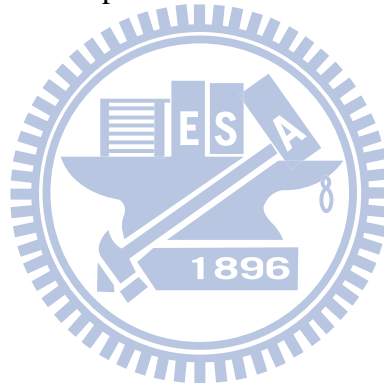
CHAPTER 4 CONCLUSIONS

A mathematical model has been developed for describing the steady-state flow caused by the constant-flux pumping in an anticline aquifer. The proposed model can account for the flow in response to partially or fully penetrating wells which are of infinitesimal diameter and with uniform inflow flux along the well screen. The anticline aquifer is homogeneous, anisotropic and confined with a shape being mimicked by three consecutive blocks. The integral transform techniques FT and FFCT are applied to derive the steady-state solutions in transform space. The coefficients in the solutions require solving a system of linear equations represented in a matrix form. Finally, the Fourier inversion is applied to obtain the drawdown solution in real space.

The present solution is applicable to simulate the flow in a slab-shaped aquifer or a hillslope aquifer by assuming two or three successive blocks are of the same height. For a slab-shaped aquifer, the simulated drawdown responses based on the present solution are identical to those evaluated by the image-well method when the well is fully penetrating and the aquifer is homogeneous, isotropic, confined and bounded by two parallel constant-head boundaries. Both the present solution and the numerical model, MODFLOW, are applied to simulate the case of flow in a hillslope aquifer. The grid settings allow MODFLOW to simulate the slope boundary in a more realistic

manner. Small differences between these simulated results can be observed around the step-like boundary. In addition, the solution is used to investigate the influence of the aquifer geometry and anisotropy as well as the well partial penetration and location on the steady-state flow pattern. The results shown in these cases exhibit significant vertical flow around the concave corner of the top boundary for a fully penetrating well or a partially penetrating well located at the hump zone of the anticline. The constant-flux pumping in a thin-limbs or narrow-ridged anticline would cause a much sharp head drop in the ridge zone. The influence of aquifer anisotropy on the observed drawdown cannot be ignored when the pumping carries out in a partially penetrating well, especially for the well of short open screen. When the screen length or/and the anisotropy ratio decreases, the dimensionless drawdown around the pumping well increases under the same constant pumping rate. In addition, we suggest using the real dimensionless screen length in the simulation even if the penetration ratio may be changed in the simplified anticline aquifer. Finally, the present solution can simulate the flow field for an arbitrarily located pumping well. Naturally the flow field will change with the location of the pumping well. The well located at the top-middle of the aquifer would produce larger drawdown around the well because of the boundary restriction on the anticline shape. The model MODFLOW, which can provide a better approximation on the curved

boundary, is employed to simulate the flow field of the anticline aquifer. The simulated results are compared with those of the present solution for the flow toward a fully penetrating well in an anticline aquifer. The present solution gives slightly higher dimensionless drawdown than the MODFLOW while the simulation is achieved by approximating the top boundary of aquifer with multiple steps. The drawdown solution derived in this study can be further applied to identify the aquifer parameters if integrated with an optimization algorithm and to do preliminary assessment for a potential waste disposal site.



REFERENCES

- Al-Mohannadi, N., Ozkan, E. and Kazemi, H., 2007. Pressure-transient responses of horizontal and curved wells in anticlines and domes. *SPE Reservoir Evaluation & Engineering*, 10(1): 66-76.
- Ashjari, J. and Raeisi, E., 2006. Influences of anticlinal structure on regional flow, Zagros, Iran. *Journal of Cave and Karst Studies*, 68(3): 118-129.
- Chan, Y.K., Mullineux, N. and Reed, J.R., 1976. Analytical solutions for drawdowns in rectangular artesian aquifers. *Journal of Hydrology*, 31: 151-160.
- Chan, Y.K., Mullineux, N., Reed, J.R. and Wells, G.G., 1978. Analytic solutions for drawdowns in wedge-shaped artesian aquifers. *Journal of Hydrology*, 36: 233-246.
- Chen, Y.J., Yeh, H.D., and Yang, S.Y., 2009. Analytical solutions for constant-flux and constant-head tests at a finite-diameter well in a wedge-shaped aquifer, *Journal of Hydraulic Engineering ASCE*, 135(4): 333-337.
- Chiang, W.H. and Kinzelbach, W., 2001. *3D-Groundwater Modeling with PMWIN: A Simulation System for Modeling Groundwater Flow and Transport Process*. Springer-Verlag Berlin Heidelberg, New York, 346 pp.
- Connell, L.D., Jayatilaka, C. and Bailey, M., 1998. A quasi-analytical solution for groundwater movement in hillslopes. *Journal of Hydrology*, 204(1-4): 108-123.

Ferris, J.G., Knowles, D.B., Brown, R.H. and Stallman, R.W., 1962. Theory of Aquifer Tests WATER-SUPPLY PAPER 1536-E, 1962, 104 P.

Harbaugh, A.W. and McDonald, M.G., 1996a. User's Documentation for MODFLOW-96, An Update to the U.S. Geological Survey Modular Finite-Difference Ground-Water Flow Model. Open-file report 96-485. U.S. Geological Survey.

Harbaugh, A.W. and McDonald, M.G., 1996b. Programmer's Documentation for MODFLOW-96, An Update to the U.S. Geological Survey Modular Finite-Difference Ground-Water Flow Model. Open-File Report 96-486. U.S. Geological Survey.

IMSL. 2003. IMSL Fortran Library User's Guide Math/Library Volume 2 of 2, version 5.0, Houston, Texas: Visual Numerics.

Javandel, I. and Zagheri, N., 1975. Analysis of flow to an extended fully penetrating well. Water Resources Research, 11(1): 159-164.

Jeffrey, A. and Dai, H.H., 2008. Handbook of Mathematical Formulas and Integrals. 4th Ed., Elsevier, 541 pp.

Kirkham, D., 1957. Potential and capacity of concentric coaxial capped cylinders. Journal of Applied Physics, 28(6): 724-731.

Kirkham, D., 1959. Exact theory of flow into a partially penetrating well. Journal of

Geophysical Research, 64(9): 1317-1327.

Kuo, M.C.T., Wang, W.L., Lin, D.S., Lin, C.C. and Chiang, C.J., 1994. An image-well method for predicting drawdown distribution in aquifers with irregularly shaped boundaries Ground Water, 32(5): 794-804.

McDonald, M.G. and Harbaugh, A.W., 1988. A Modular Three-Dimensional Finite-Difference Ground-Water Flow Model. Book 6, Chapter A1, Open-file report 83-875, U.S. Geological Survey.

Shanks, D., 1955. Non-linear transformations of divergent and slowly convergent sequences. Journal of Mathematics and Physics, 34: 1-42.

Streltsova, T.D., 1988. Well Testing in Heterogeneous Formations. John Wiley & Sons, New York, 413 pp.

Theis, C.V., 1935. The relation between the lowering of the piezometric surface and the rate and duration of discharge of a well using groundwater storage. Trans. Amer. Geophys. Union, 16(1): 519-524.

Thiem, G., 1906. Hydrologische Methoden, JM Gephardt, Leipzig.

Yeh, H.D. and Chang, Y.C., 2006. New analytical solutions for groundwater flow in wedge-shaped aquifers with various topographic boundary conditions. Advances in Water Resources, 29(3): 471-480.

Yeh, H.D. and Kuo, C.C., 2010. An analytical solution for heterogeneous and

anisotropic anticline reservoirs under well injection. *Advances in Water Resources*, 33(4): 419-429.



APPENDIX A DERIVATION OF EQ. (22)

This appendix demonstrates the procedure for obtaining Eq. (22). Taking FT and FFCT to Eq. (10) with boundary conditions (11) to (14) results in

$$\frac{d^2 \hat{s}_{D2}}{dx_D^2} - (\varepsilon^2 \chi_{yx} + \omega_n^2 \chi_{zx}) \hat{s}_{D2} = 0, \quad x_{Da1P} \leq x_D \leq x_{Da2} \quad (A1)$$

with ε and ω_n represent the transform variables in relation to y_D and z_D , respectively. The solution for the ODE is

$$\hat{s}_{D2n}(x_D) = P_1 \exp(\alpha_n x_D) + P_2 \exp(-\alpha_n x_D) \quad (A2)$$

where α_n is defined by Eq. (24); P_1 and P_2 are the coefficients needed to be determined by conditions (6a), (7), and (15). If one takes the inversion of FFCT to Eq. (A2), the solution in Fourier domain is

$$\begin{aligned} \bar{s}_{D2}(x_D, z_D) = & \frac{1}{z_{Db2}} [P_{10} \exp(\alpha_0 x_D) + P_{20} \exp(-\alpha_0 x_D)] \\ & + \frac{2}{z_{Db2}} \sum_{n=1}^{\infty} [P_{1n} \exp(\alpha_n x_D) + P_{2n} \exp(-\alpha_n x_D)] \cos(\omega_n z_D) \end{aligned} \quad (A3)$$

Eq. (A3) represents the drawdown solution for zone 2 in the Fourier domain. Eq. (22) is expressed by new coefficients in the Fourier series, which are obtained by inserting Eqs. (7) and (15) into (A3) and applying the inversion formula of the FFCT. Similar procedure can be taken for deriving Eq. (26), i.e., the drawdown solution for zone 3 in the Fourier domain. Note that ζ_k defined in Eq. (26) is chosen as the transform variable when applying FFCT over the interval $[0, z_{Db3}]$.

APPENDIX B MATRIX FORMULATION FOR SOLVING COEFFICIENTS

The coefficients V_0 , V_n , W_0 and W_k in Eqs. (22), (26), (38), and (39)

construct a system of $i + j + 2$ linear equations, which can be expressed in matrix

form as

$$\begin{bmatrix} 1+D_{00} & D_{01} & D_{02} & \dots & D_{0i} & E_{00} & E_{01} & E_{02} & \dots & E_{0j} \\ D_{10} & 1+D_{11} & D_{12} & \dots & D_{1i} & E_{10} & E_{11} & E_{12} & \dots & E_{1j} \\ D_{20} & D_{21} & 1+D_{22} & \dots & D_{2i} & E_{20} & E_{21} & E_{22} & \dots & E_{2j} \\ \vdots & \vdots & \vdots & \vdots & \vdots & \vdots & \vdots & \vdots & \dots & \vdots \\ D_{n0} & D_{n1} & D_{n2} & \dots & 1+D_{ni} & E_{n0} & E_{n1} & E_{n2} & \dots & E_{nj} \\ F_{00} & F_{01} & F_{02} & \dots & F_{0i} & 1+G_{00} & G_{01} & G_{02} & \dots & G_{0j} \\ F_{10} & F_{11} & F_{12} & \dots & F_{1i} & G_{10} & 1+G_{11} & G_{12} & \dots & G_{1j} \\ F_{20} & F_{21} & F_{22} & \dots & F_{2i} & G_{20} & G_{21} & 1+G_{22} & \dots & G_{2j} \\ \vdots & \vdots & \vdots & \vdots & \vdots & \vdots & \vdots & \vdots & \dots & \vdots \\ F_{k0} & F_{k1} & F_{k2} & \dots & F_{ki} & G_{k0} & G_{k1} & G_{k2} & \dots & 1+G_{kj} \end{bmatrix} \begin{bmatrix} V_0 \\ V_1 \\ V_2 \\ \vdots \\ V_i \\ W_0 \\ W_1 \\ W_2 \\ \vdots \\ W_j \end{bmatrix} = \begin{bmatrix} S_0 \\ S_1 \\ S_2 \\ \vdots \\ S_n \\ T_0 \\ T_1 \\ T_2 \\ \vdots \\ T_k \end{bmatrix} \quad (\text{B1})$$

with the elements

$$D_{00} = z_{Db2} \alpha_0 C_{30} \left\{ \frac{1}{\gamma_0} C_{80} + \sum_{m=1}^{\infty} \frac{2 \sin^2(\lambda_m z_{Db2})}{\gamma_m \lambda_m^2 z_{Db2}^2} C_{8m} \right\} \quad (\text{B2})$$

$$D_{0i} = \alpha_i C_{3i} \sum_{m=1}^{\infty} \frac{2 \phi(m, i) \sin(\lambda_m z_{Db2})}{\gamma_m \lambda_m z_{Db2}} C_{8m} \quad (\text{B3})$$

$$D_{n0} = \alpha_0 C_{30} \sum_{m=1}^{\infty} \frac{4 \phi(m, n) \sin(\lambda_m z_{Db2})}{\gamma_m \lambda_m z_{Db2}} C_{8m} \quad (\text{B4})$$

$$D_{ni} = \alpha_i C_{3i} \sum_{m=1}^{\infty} \frac{4 \phi(m, n) \phi(m, i)}{\gamma_m z_{Db2}} C_{8m} \quad (\text{B5})$$

$$E_{00} = -z_{Db3} \beta_0 C_{50} \left\{ \frac{1}{\gamma_0} C_{90} + \sum_{m=1}^{\infty} \frac{2 \sin(\lambda_m z_{Db2}) \sin(\lambda_m z_{Db3})}{\gamma_m \lambda_m^2 z_{Db2} z_{Db3}} C_{9m} \right\} \quad (\text{B6})$$

$$E_{0j} = -\beta_j C_{5j} \sum_{m=1}^{\infty} \frac{2 \mathcal{G}(m, j) \sin(\lambda_m z_{Db2})}{\gamma_m \lambda_m z_{Db2}} C_{9m} \quad (\text{B7})$$

$$E_{n0} = -\beta_0 C_{50} \sum_{m=1}^{\infty} \frac{4 \phi(m, n) \sin(\lambda_m z_{Db3})}{\gamma_m \lambda_m z_{Db2}} C_{9m} \quad (\text{B8})$$

$$E_{nj} = -\sum_{j=1}^{\infty} \beta_j C_{5j} \sum_{m=1}^{\infty} \frac{4\phi(m,n)\mathcal{G}(m,j)}{\gamma_m z_{Db2}} C_{9m} \quad (\text{B9})$$

$$F_{00} = z_{Db2} \alpha_0 C_{30} \left\{ \frac{1}{\gamma_0} C_{90} + \sum_{m=1}^{\infty} \frac{2 \sin(\lambda_m z_{Db2}) \sin(\lambda_m z_{Db3})}{\gamma_m \lambda_m^2 z_{Db2} z_{Db3}} C_{9m} \right\} \quad (\text{B10})$$

$$F_{0i} = \alpha_i C_{3i} \sum_{m=1}^{\infty} \frac{2\phi(m,i) \sin(\lambda_m z_{Db3})}{\gamma_m \lambda_m z_{Db3}} C_{9m} \quad (\text{B11})$$

$$F_{k0} = \alpha_0 C_{30} \sum_{m=1}^{\infty} \frac{4\mathcal{G}(m,k) \sin(\lambda_m z_{Db2})}{\gamma_m \lambda_m z_{Db3}} C_{9m} \quad (\text{B12})$$

$$F_{ki} = \alpha_i C_{3i} \sum_{m=1}^{\infty} \frac{4\mathcal{G}(m,k)\phi(m,i)}{\gamma_m z_{Db3}} C_{9m} \quad (\text{B13})$$

$$G_{00} = -z_{Db3} \beta_0 C_{50} \left\{ \frac{1}{\gamma_0} C_{80} + \sum_{m=1}^{\infty} \frac{2 \sin^2(\lambda_m z_{Db3})}{\gamma_m \lambda_m^2 z_{Db3}^2} C_{8m} \right\} \quad (\text{B14})$$

$$G_{0j} = -\beta_j C_{5j} \sum_{m=1}^{\infty} \frac{2\mathcal{G}(m,j) \sin(\lambda_m z_{Db3})}{\gamma_m \lambda_m z_{Db3}} C_{8m} \quad (\text{B15})$$

$$G_{k0} = -\beta_0 C_{50} \sum_{m=1}^{\infty} \frac{4\mathcal{G}(m,k) \sin(\lambda_m z_{Db3})}{\gamma_m \lambda_m z_{Db3}} C_{8m} \quad (\text{B16})$$

$$G_{kj} = -\beta_j C_{5j} \sum_{m=1}^{\infty} \frac{4\mathcal{G}(m,k)\mathcal{G}(m,j)}{\gamma_m z_{Db3}} C_{8m} \quad (\text{B17})$$

$$S_0 = \frac{q_D U_{c0}}{\gamma_0} C_{10}(x_{Da1P}) + \sum_{m=1}^{\infty} \frac{2q_D U_{cm} \sin(\lambda_m z_{Db2})}{\gamma_m \lambda_m z_{Db2}} C_{1m}(x_{Da1P}) \quad (\text{B18})$$

$$S_n = \sum_{m=1}^{\infty} \frac{4q_D U_{cm} \phi(m,n)}{\gamma_m z_{Db2}} C_{1m}(x_{Da1P}) \quad (\text{B19})$$

$$T_0 = \frac{q_D U_{c0}}{\gamma_0} C_{10}(x_{Da1N}) + \sum_{m=1}^{\infty} \frac{2q_D U_{cm} \sin(\lambda_m z_{Db3})}{\gamma_m \lambda_m z_{Db3}} C_{1m}(x_{Da1N}) \quad (\text{B20})$$

and

$$T_k = \sum_{m=1}^{\infty} \frac{4q_D U_{cm} \mathcal{G}(m,k)}{\gamma_m z_{Db3}} C_{1m}(x_{Da1N}) \quad (\text{B21})$$

where

$$C_{8m} = \coth[\gamma_m (x_{Da1P} - x_{Da1N})], \quad m = 0, 1, 2, 3, \dots \quad (\text{B22})$$

and

$$C_{9m} = \text{csch}[\gamma_m (x_{Da1P} - x_{Da1N})], \quad m = 0, 1, 2, 3, \dots \quad (\text{B23})$$

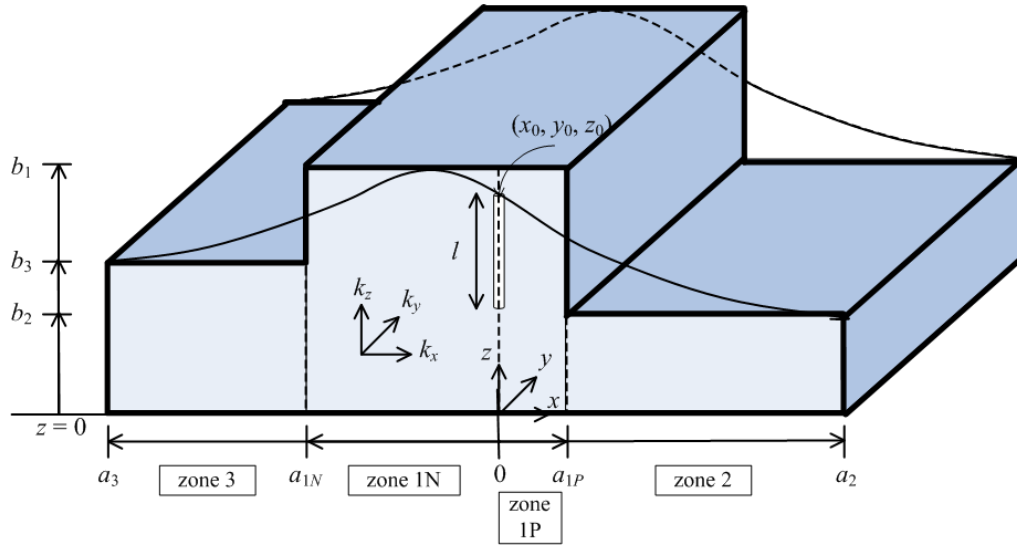
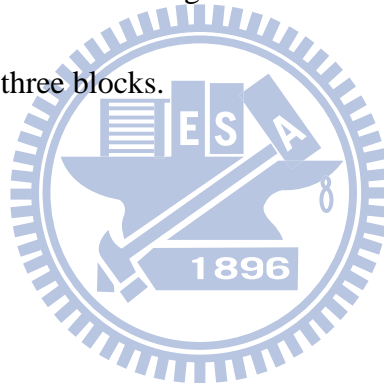


Figure 1. Schematic representation of a groundwater flow problem in an anticline aquifer with a line sink located along the z axis. The anticline aquifer is approximately divided into three blocks.



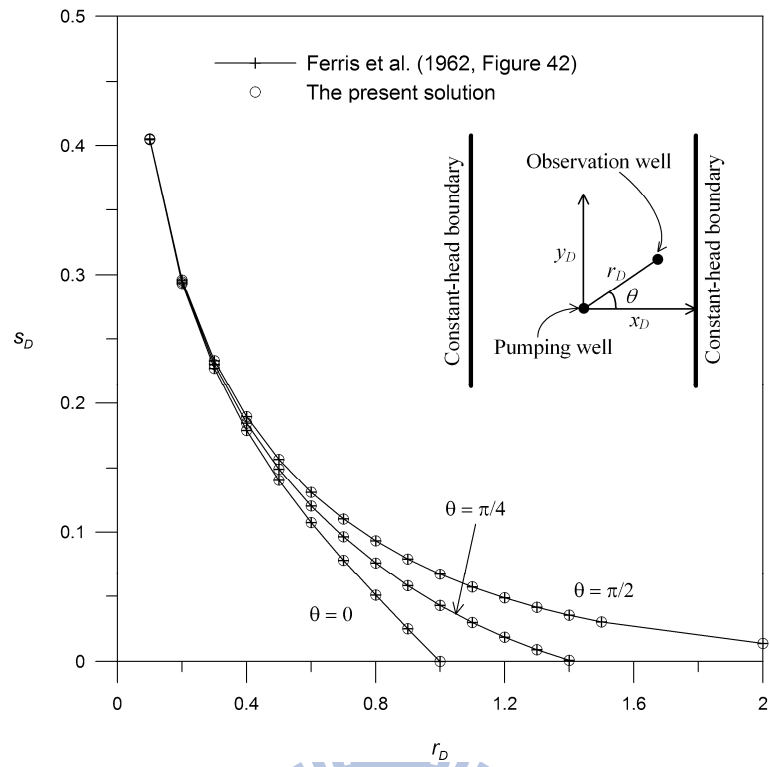


Figure 2. The dimensionless drawdown distributions predicted by the present solution and the image-well method (Ferris et al., 1962) for pumping at the middle of a slab-shaped aquifer bounded by two parallel constant-head boundaries.

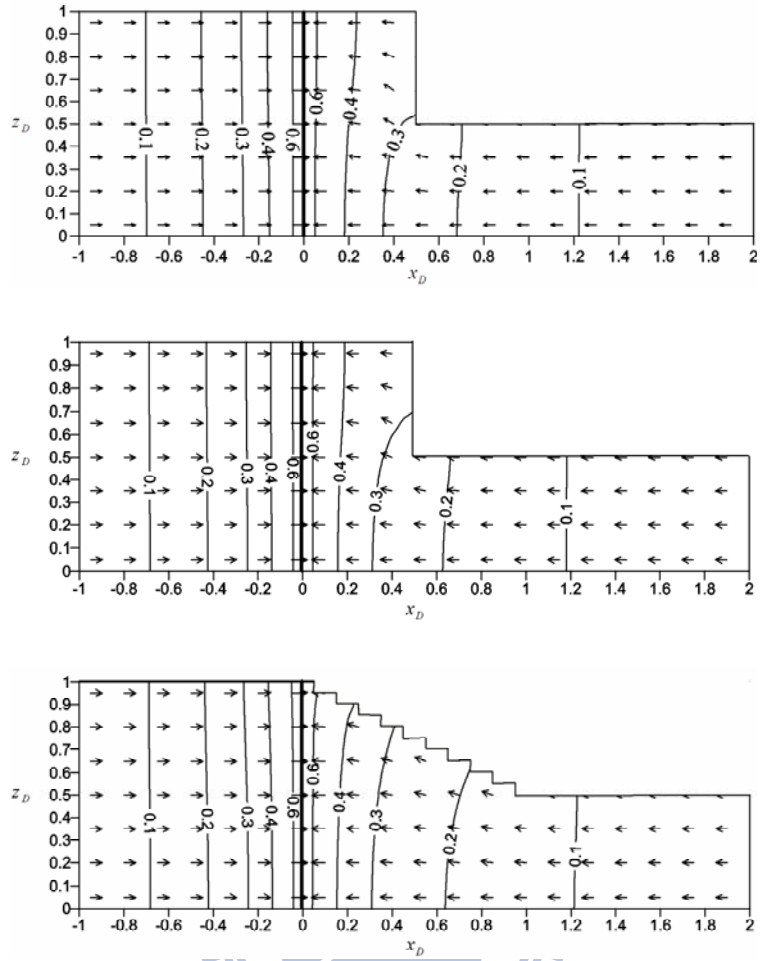


Figure 3. Dimensionless drawdown contours and flow field for the pumping at a fully penetrating well in a hillslope aquifer. The simulations were carried out to a step-like aquifer by (a) the present solution, (b) MODFLOW, (c) MODFLOW with multiple steps to approximate the inclined boundary.

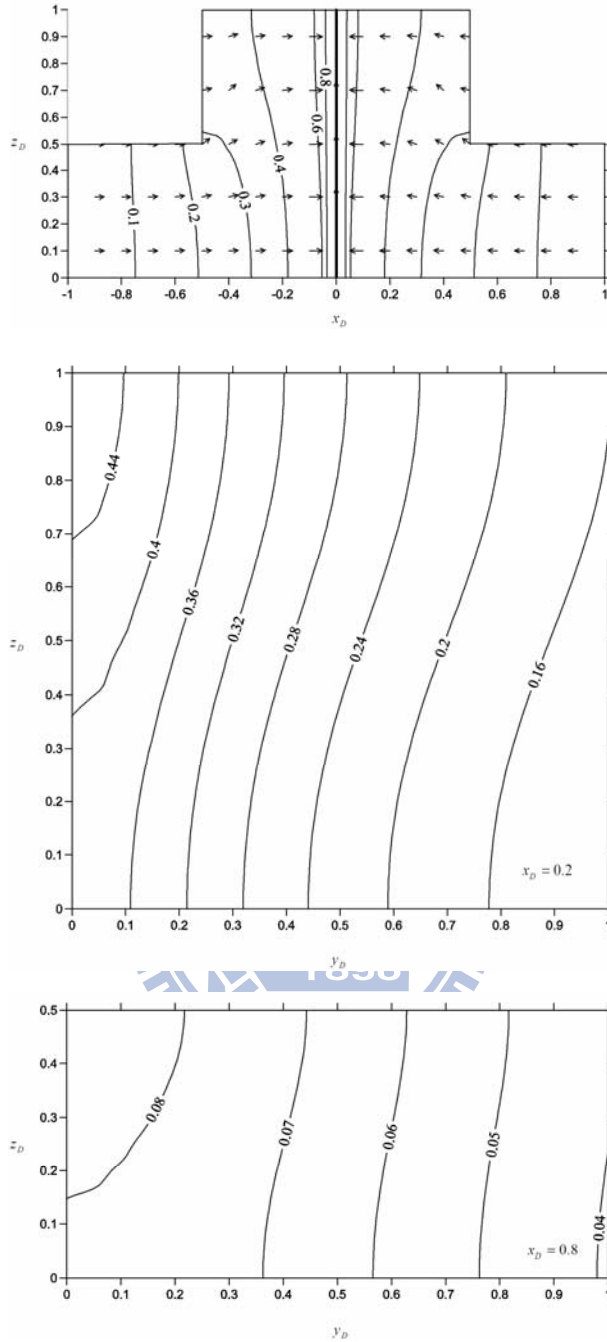


Figure 4. Dimensionless drawdown contours produced by the present solution for the pumping at a fully penetrating well in an isotropic anticline aquifer. The cross-sectional view on (a) $x_D - z_D$ plane for $y_D = 0$, (b) $y_D - z_D$ plane for $x_D = 0.2$, and (c) $y_D - z_D$ plane for $x_D = 0.8$.

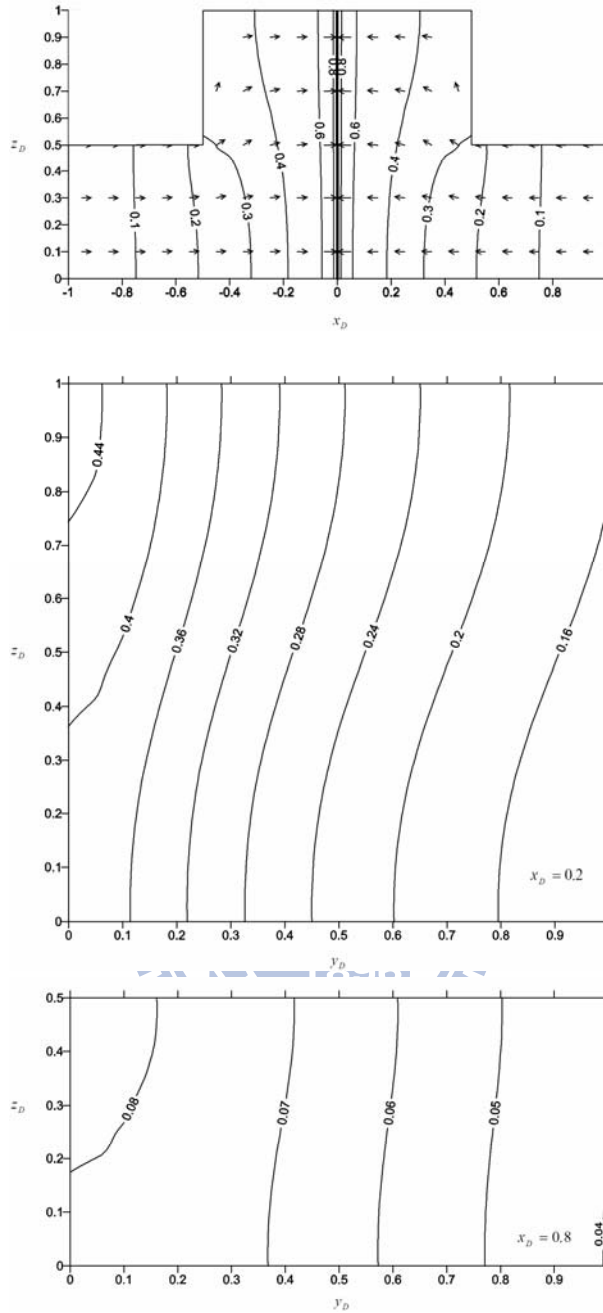


Figure 5. Dimensionless drawdown contours produced by MODFLOW for the pumping at a fully penetrating well in an isotropic anticline aquifer. The applied aquifer geometry is the same as that in Figure 4. The cross-sectional view on (a) $x_D - z_D$ plane for $y_D = 0$, (b) $y_D - z_D$ plane for $x_D = 0.2$, and (c) $y_D - z_D$ plane for $x_D = 0.8$.

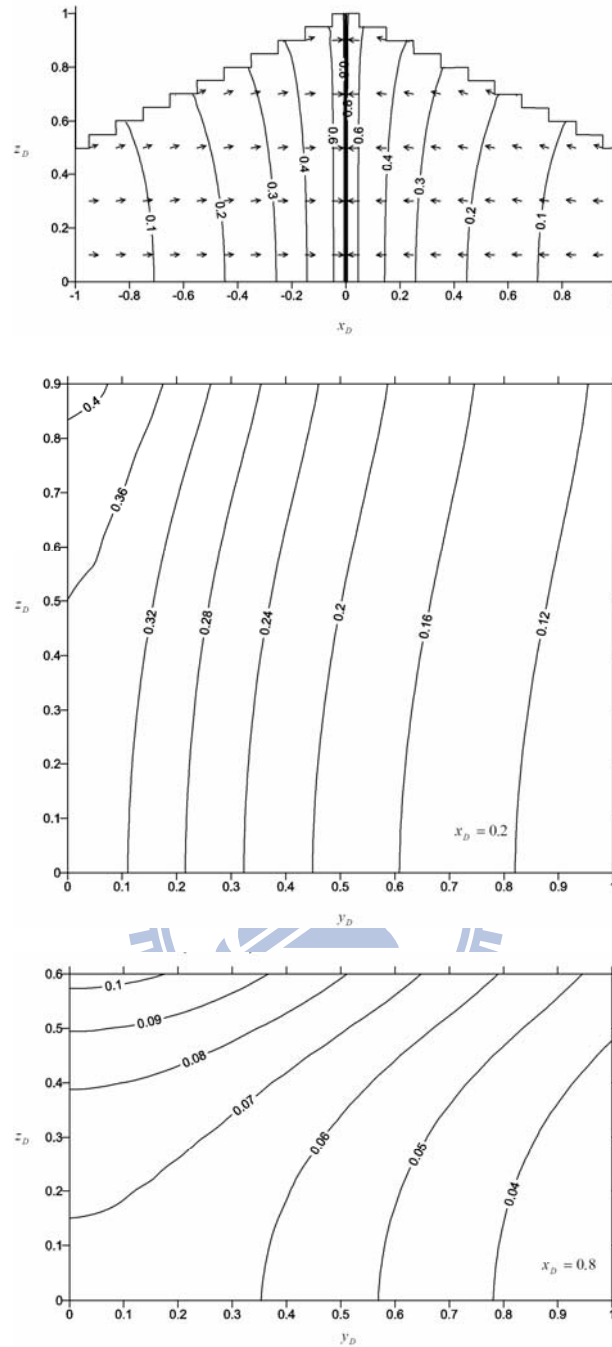


Figure 6. Dimensionless drawdown contours produced by MODFLOW for the pumping at a fully penetrating well in an isotropic anticline aquifer. The upper boundary of anticline aquifer is approximated by multiple steps. The cross-sectional view on (a) $x_D - z_D$ plane for $y_D = 0$, (b) $y_D - z_D$ plane for $x_D = 0.2$, and (c) $y_D - z_D$ plane for $x_D = 0.8$.

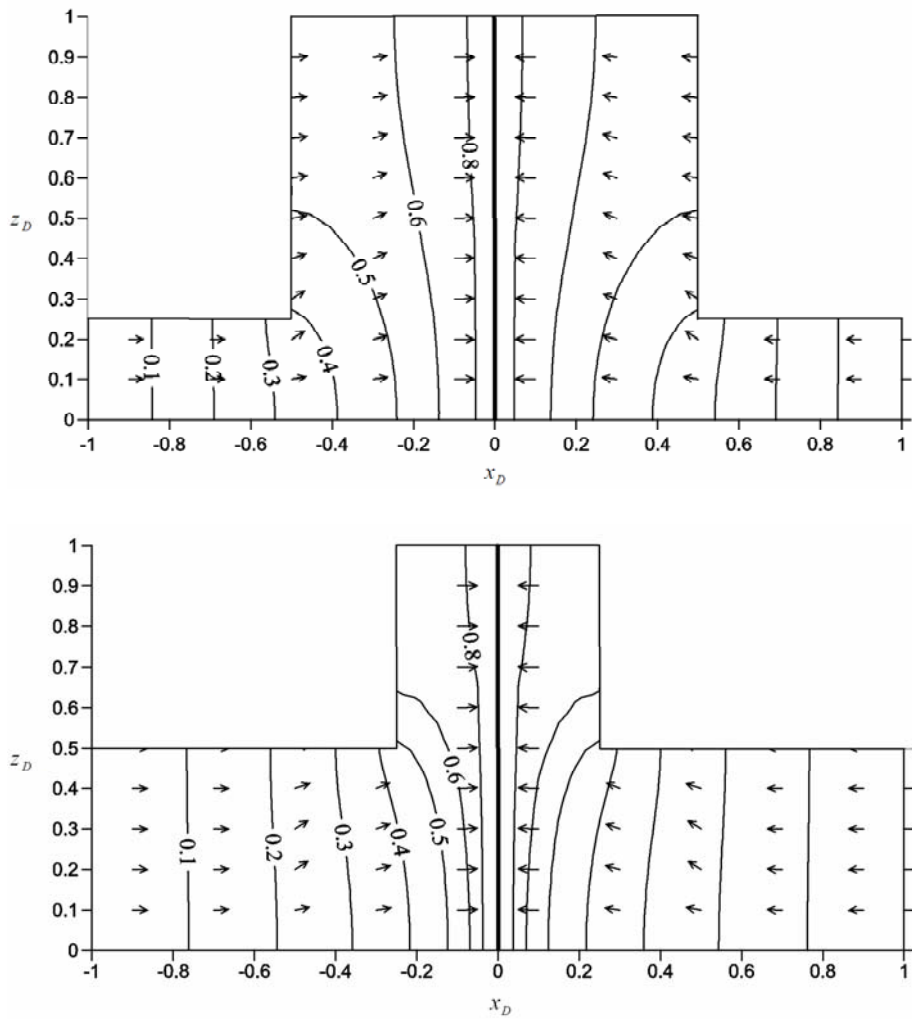


Figure 7. Plots of dimensionless drawdown contours and flow fields for pumping at a fully penetrating well in an isotropic aquifer of (a) thin limbs and (b) narrow ridge.

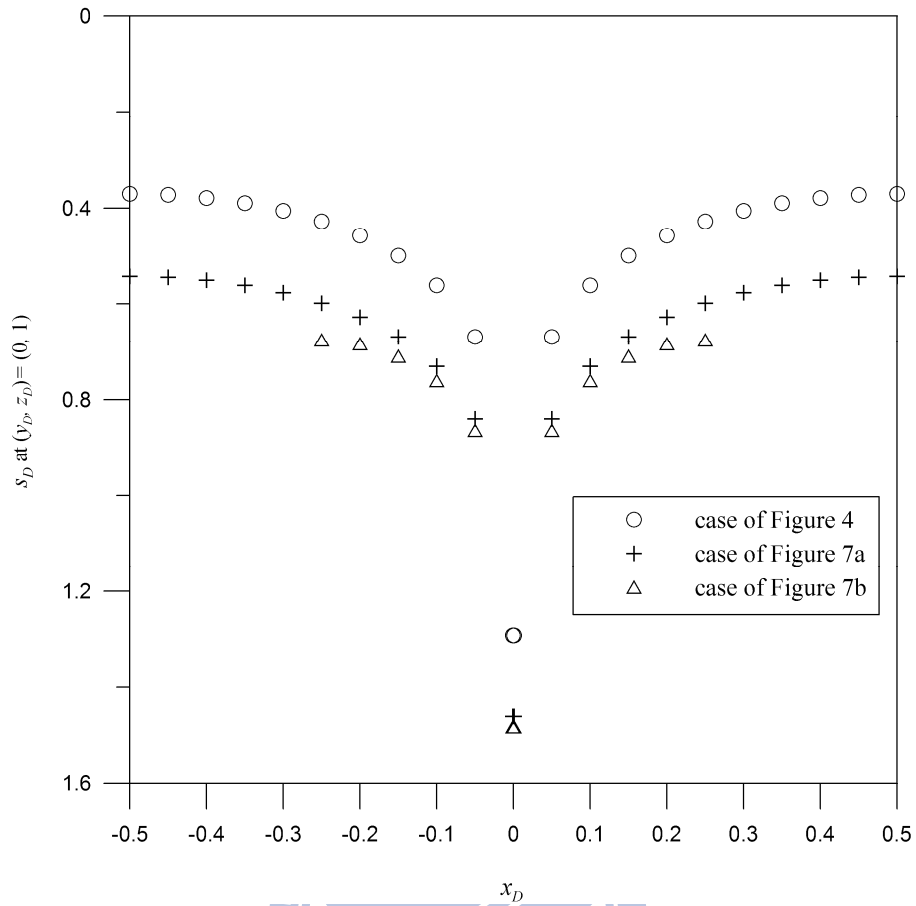


Figure 8. Dimensionless drawdown responses versus x_D calculated at $(y_D, z_D) = (0, 1)$ for the base case shown in Figure 4 and the cases investigated in Figure 7.

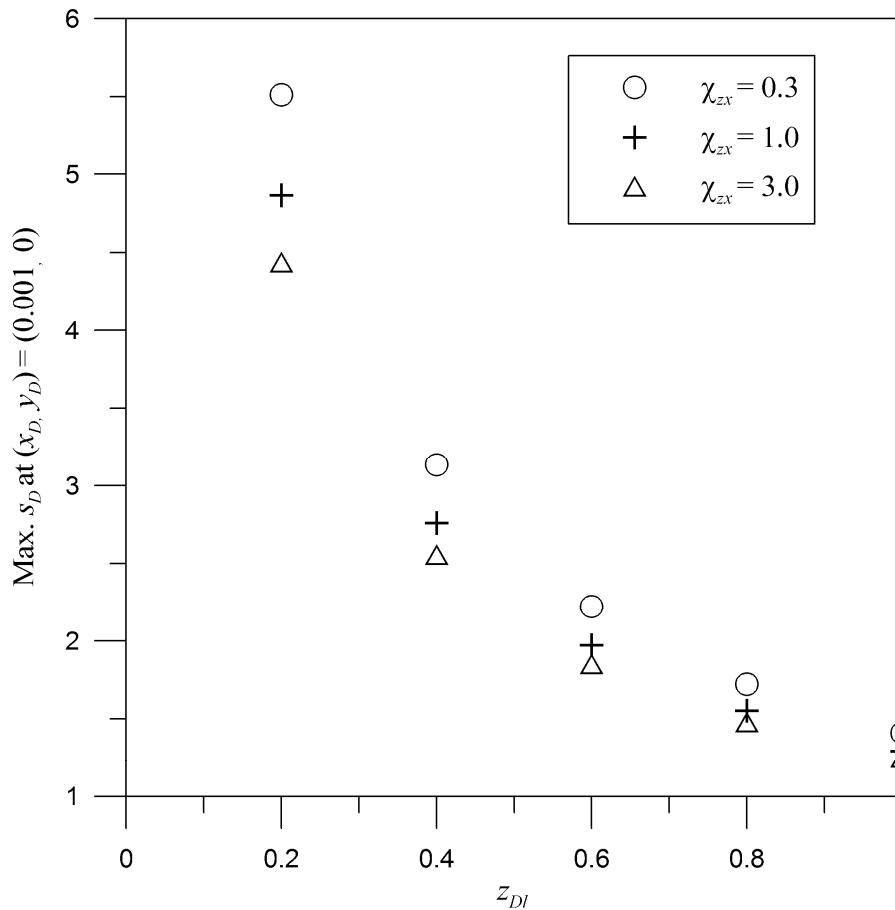


Figure 9. A comparison of largest dimensionless drawdown at $(x_D, y_D) = (0.001, 0)$ for the cases of different screen length and aquifer anisotropy ratios. The wells are screened from the top-middle of the anticline aquifer. The geometry of the aquifer is the same as the base case shown in Figure 4.

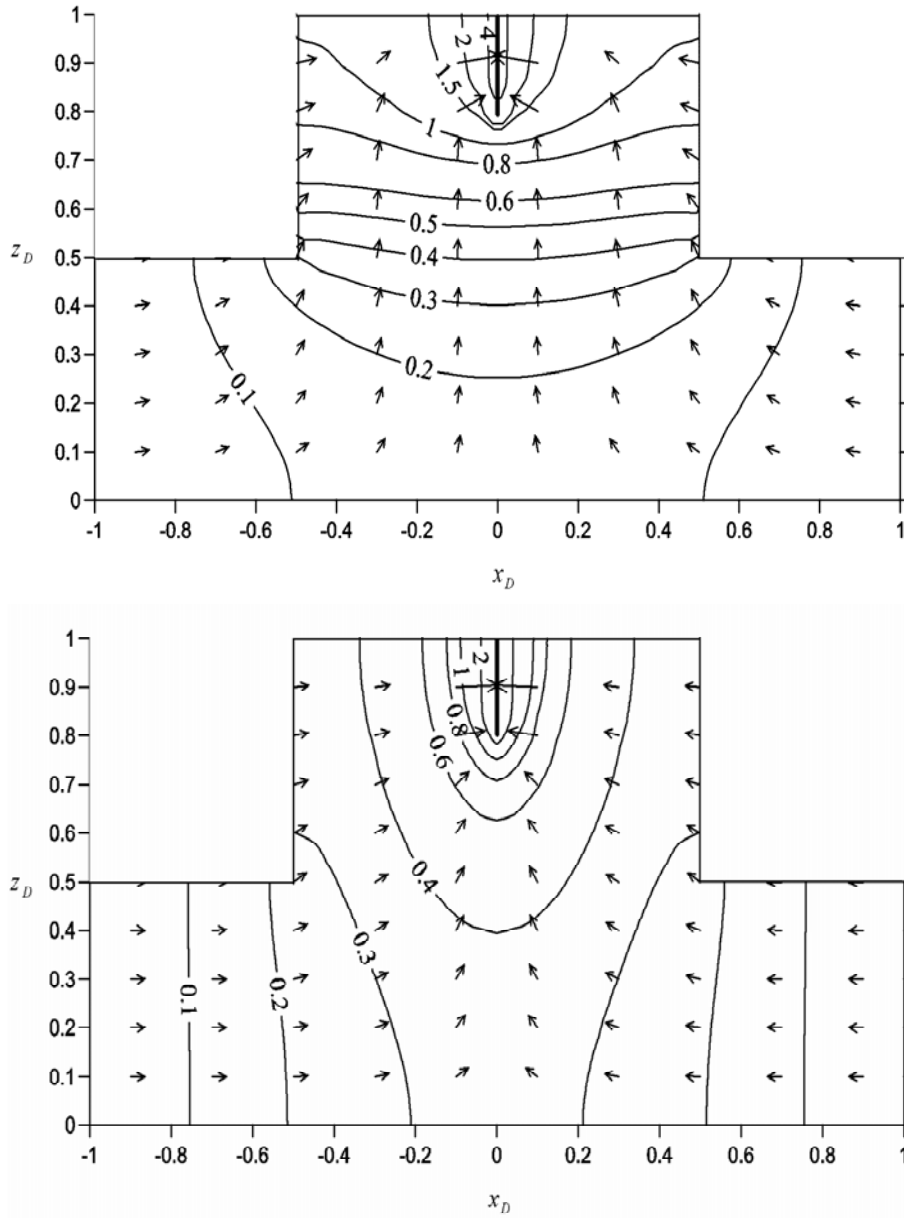


Figure 10. Plots of dimensionless drawdown contours and flow fields for the pumping at a partially penetrating well in the aquifers with the anisotropy ratios of (a) $\chi_{zx} = 0.3$ and (b) $\chi_{zx} = 3$. The dimensionless screen length of the pumping well is 0.2.

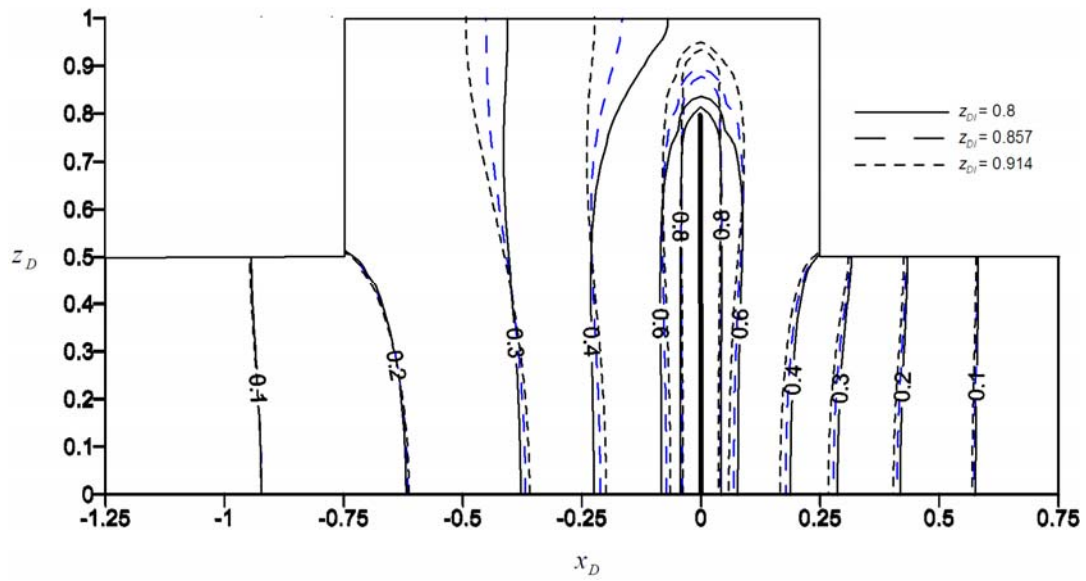


Figure 11. Plots of dimensionless drawdown contours for the pumping at partially penetrating wells in an aquifer with the dimensionless screen lengths of (a) $z_{Dl} = 0.8$, (b) $z_{Dl} = 0.857$ and (c) $z_{Dl} = 0.914$. The wells are located at a dimensionless x_D distance of 0.25 from the midline of the anticline aquifer.

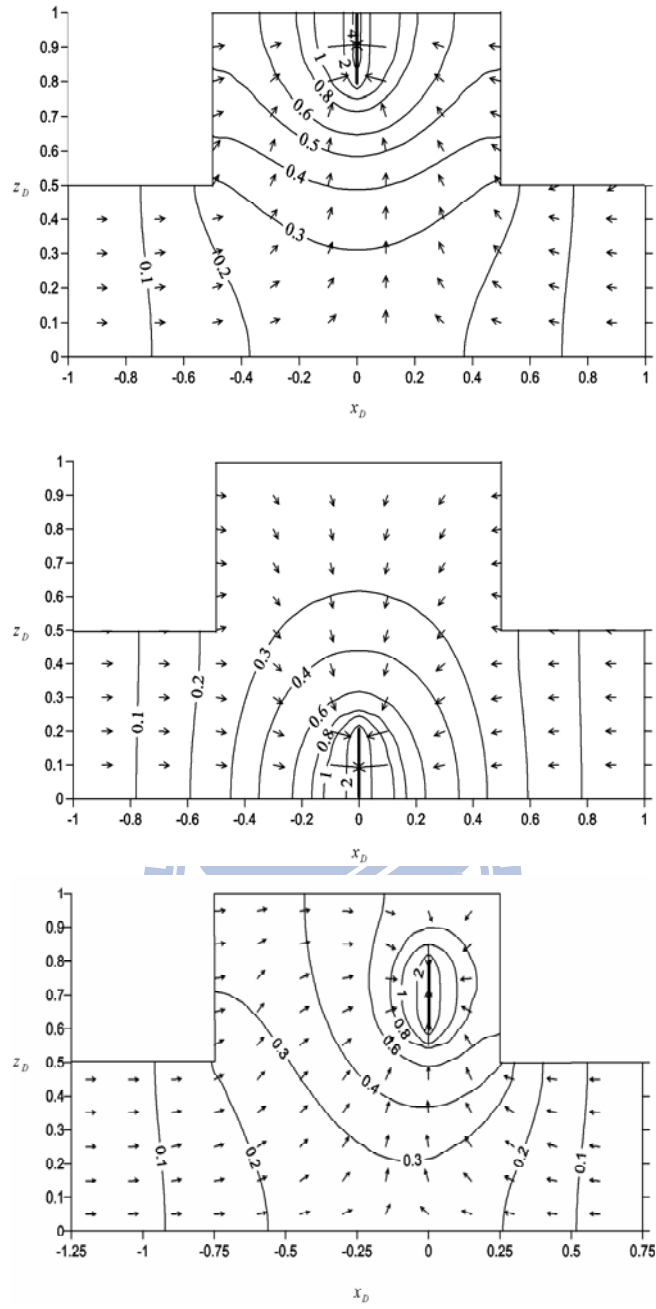


Figure 12. Plots of dimensionless drawdown contours and flow fields for the pumping at a partially penetrating well with the dimensionless screen length of 0.2. The wells are located at (a) $z_{0D} = 1.0$ and (b) $z_{0D} = 0.2$ on the midline of the anticline aquifer and (c) $z_{0D} = 0.8$ at a dimensionless x_D distance of 0.25 from the midline of the anticline aquifer.

VITA (作者簡歷)

姓 名 陳彥如 (Yen-Ju Chen)

出生日期 民國 70 年 10 月 5 日

學 歷 88.09-92.06 學士，私立東海大學環境科學系

92.09-94.06 碩士，國立交通大學環境工程研究所

94.09-99.08 國立交通大學環境工程研究所博士班

通訊電話 03-5712121 # 55526

行動電話 0915-219990

地 址 408 台中市南屯區黎明東街 368 號 7 樓

電子郵件 yenju.ev92g@nctu.edu.tw



PUBLICATION LIST

期刊論文

1. Yeh, H. D., S. Y. Yang, and Y. J. Chen, 2007. Discussion of “Approximate Discharge for Constant Head Test with Recharging Boundary” by Philippe Renard, *Ground Water*, 45(6), 659, doi: 10.1111/j.1745-6584.2007.00386. (SCI)
2. Yeh, H. D. and Y. J. Chen. (2007). Determination of skin and aquifer parameters for a slug test with wellbore-skin effect, *Journal of Hydrology*, 342, 283-294. (SCI)
3. Chen, Y. J., H. D. Yeh, and S. Y. Yang, 2007. A new semi-analytical solution for slug test in a confined aquifer under the effects of well partial penetration, *Journal of Hydroscience and Hydraulic Engineering, JSCE*, 25(2), 59-74.
4. Yeh, H. D., Y. J. Chen, and S. Y. Yang, 2008. Semi-analytical solution for a slug test in partially penetrating wells including the effect of finite-thickness skin, *Hydrological Processes*, 22, 3741-3748. (SCI)
5. Chen, Y. J., and H. D. Yeh, 2009. Parameter estimation/sensitivity analysis for an aquifer test with skin effect, *Ground Water*, 47(2), 287-299. (SCI)
6. Chen, Y. J., H. D. Yeh, and S. Y. Yang, 2009. Analytical solutions for constant-flux and constant-head tests at a finite-diameter well in a wedge-shaped aquifer, *Journal of Hydraulic Engineering ASCE*, 135(4), 333-337, doi: 10.1061/_ASCE_0733-9429. (SCI)
7. Yeh, H. D., and C. H. Chang, Y. J. Chen, 2009. Aquifer parameter estimation for a constant-flux test performed in a radial two-zone aquifer, *Journal of Irrigation and Drainage Engineering ASCE*, 135(5), 693-703, doi: 10.1061/(ASCE)IR.1943-4774.0000064. (SCI)
8. Yeh, H. D., and Y. J. Chen, 2009. Comment on “Utilization of Weibull techniques for short-term data analysis in environmental engineering,” by Isaiah A. Oke, 2008, 25(7), 1099–1106. *Environmental Engineering Science*, 26(8), 1365-1367. doi:10.1089/ees.2008.0374. (SCI)

研討會論文

1. 陳彥如、楊紹洋、葉弘德，93年7月，微水試驗在受限含水層和部分貫穿井影響下的半解析解，第十四屆水利工程研討會，國立交通大學，新竹市，論文集(下冊)F164-F169頁。
2. 陳彥如、葉弘德、楊紹洋，93年10月，微水試驗在井膚層及部分貫穿井效應下的半解析解，九十三年度農業工程研討會，中國農業工程學會，桃園，論文摘要集243頁，論文集光碟版1507-1514頁。
3. 陳彥如、葉弘德，95年7月，微水試驗的井膚層厚度及水層參數推求，第十五屆水利工程研討會，國立中央大學，中壢市，論文集(上冊)E126-E131頁。

4. 陳彥如、葉弘德、楊紹洋，95年10月，考慮井徑的定流量試驗在鄰近地形邊界的解析解，九十五年度農業工程研討會，中國農業工程學會，台南市，論文摘要集91頁，論文集光碟版280-290頁。
5. 陳彥如、葉弘德、楊紹洋，95年11月，考慮井徑的定水頭試驗在楔型含水層的解析解，2006土壤與地下水研討會，中國環境工程學會，台中市，論文摘要集507頁，論文集光碟版Soi20060060.pdf。(優秀論文獎)
6. Chen, Y.J., H.D. Yeh, and S.Y. Yang, 2007. New solutions for constant-flux and constant-head tests in a wedge-shaped aquifer. Asia Oceania Geosciences Society (AOGS) 4th Annual Meeting, Bangkok, Thailand, HS05-A0002.
7. 陳彥如、葉弘德，97年10月，定水頭試驗數據對於水文地質參數的敏感度與在參數估計上的影響，九十七年度農業工程研討會，中國農業工程學會，台北市，論文摘要集95頁，論文集光碟版265-274頁。
8. Chen, Y.J. and H.D. Yeh, 2009. Composite analysis of test-well and observation-well data during constant-head test. 7th Symposium on Groundwater, Hydrology, Quality, and Management, World Environmental and Water Resources Congress 2009, Kansas City, Missouri, 2014-2021.
9. 陳庚轅、陳彥如、葉弘德、Dong-Sheng Jeng，98年9月，利用濱海觀測井水位變化推求海岸坡度與含水層參數，九十八年電子計算機於土木水利工程應用論文研討會，中華大學，新竹市，論文集869-973頁。
10. 陳彥如、葉弘德、郭嘉真，98年12月，在背斜含水層進行定流量抽水之洩降分佈，第七屆地下水資源及水質保護研討會，台灣大學，台北市，論文集A-1-A-7頁。
11. 葉弘德、陳彥如，98年12月，低放射性廢棄物核種全系統安全評估模式之重要參數敏感度分析，第七屆地下水資源及水質保護研討會，台灣大學，台北市，論文集L-1-L-6頁。
12. 陳彥如、葉弘德，98年12月，低放射性廢棄物處置場全系統安全評估程式及重要參數之分析研究，行政院原能會委託研究計畫暨國科會與原能會科技學術合作研究計畫成果發表會，核能研究所，桃園縣，摘要集E-3頁。